CANCER

A Validated Tumorgraft Model Reveals Activity of Dovitinib Against Renal Cell Carcinoma

Sharanya Sivanand,[1,2,3] Samuel Peña-Llopis,[1,2,3] Hong Zhao,[3] Blanka Kucejova,[1,2,3] Patrick Spence,[1,2,3] Andrea Pavia-Jimenez,[1,2,3] Toshinari Yamasaki,[1,2,3] David J. McBride,[4] Jessica Gillen,[1,2,3] Nicholas C. Wolff,[1,2,3] Lorraine Morlock,[5] Yair Lotan,[6] Ganesh V. Raj,[6] Arthur Sagalowsky,[6] Vitaly Margulis,[6] Jeffrey A. Cadeddu,[6] Mark T. Ross,[4] David R. Bentley,[4] Wareef Kabbani,[7] Xian-Jin Xie,[3] Payal Kapur,[7] Noelle S. Williams,[5] James Brugarolas[1,2,3]*

Most anticancer drugs entering clinical trials fail to achieve approval from the U.S. Food and Drug Administration. Drug development is hampered by the lack of preclinical models with therapeutic predictive value. Herein, we report the development and validation of a tumorgraft model of renal cell carcinoma (RCC) and its application to the evaluation of an experimental drug. Tumor samples from 94 patients were implanted in the kidneys of mice without additives or disaggregation. Tumors from 35 of these patients formed tumorgrafts, and 16 stable lines were established. Samples from metastatic sites engrafted at higher frequency than those from primary tumors, and stable engraftment of primary tumors in mice correlated with decreased patient survival. Tumorgrafts retained the histology, gene expression, DNA copy number alterations, and more than 90% of the protein-coding gene mutations of the corresponding tumors. As determined by the induction of hypercalcemia in tumorgraft-bearing mice, tumorgrafts retained the ability to induce paraneoplastic syndromes. In studies simulating drug exposures in patients, RCC tumorgraft growth was inhibited by sunitinib and sirolimus (the active metabolite of temsirolimus in humans), but not by erlotinib, which was used as a control. Dovitinib, a drug in clinical development, showed greater activity than sunitinib and sirolimus. The routine incorporation of models recapitulating the molecular genetics and drug sensitivities of human tumors into preclinical programs has the potential to improve oncology drug development.

INTRODUCTION

More than 80% of anticancer drugs administered to patients in clinical trials fail to reach U.S. Food and Drug Administration (FDA) approval (*1*–*3*), twice the failure rate of drugs in other categories (*1*). Better paradigms and preclinical models are needed to reduce the toll on patient lives and resources.

Most preclinical studies evaluate drugs by testing them in tumor cell lines that have been passaged in culture for many years (for example, the NCI-60 panel) (*4*, *5*). Although these cell lines have been very useful, their value is diminished by new mutations acquired during adaptation to growth in culture and subsequent expansion (*6*, *7*). In addition, tumors formed by cell lines in mice tend to be poorly differentiated and likely dissimilar from the tumor from which the cell line was originally derived (*6*–*9*). These factors probably explain their limited use in predicting drug responsiveness in patients.

Renal cell carcinoma (RCC) is especially well suited for the development of a tumorgraft model in which tumors derived from patients are implanted in mice. First, RCCs are typically large, providing access to abundant tumor material. Second, RCC is seldom treated with chemotherapy, and thus, the molecular genetics and behavior of the tumor is unlikely to be affected by previous exposure to DNA damaging agents. Third, RCCs implanted in mice preserve the histology and karyotype of patient tumors (*10*–*16*). Fourth, the implantation of tumors heterotopically in mice may affect tumor biology (*17*–*19*), but the site for orthotopic implantation of RCC, under the kidney capsule, is a privileged site for tumor growth (*4*). Finally, because RCC is usually treated with molecularly targeted medicines, an RCC tumorgraft model would permit testing the model with this emerging class of drugs.

Most patients with unresectable RCC are treated with angiogenesis inhibitors and inhibitors of mammalian target of rapamycin complex 1 (mTORC1) (*20*). RCC of clear-cell type (ccRCC) accounts for 70% of all RCC (*21*) and is characterized by inactivation of the tumor suppressor gene von Hippel–Lindau (*VHL*) (*22*). *VHL* inactivation results in constitutive activation of hypoxia-inducible factor (HIF) and consequent induction of vascular endothelial growth factor (*VEGF*) and platelet-derived growth factor β (*PDGF*β) (*23*, *24*). VEGF acts on VEGF receptor 2 (VEGFR2) on endothelial cells (*25*) and PDGFβ acts on PDGF receptor β (PDGFRβ) on pericytes, thereby promoting angiogenesis (*26*). These findings paved the way for the development of a VEGF-neutralizing antibody, bevacizumab (*27*–*30*), and of several inhibitors targeting both VEGFR2 and PDGFRβ—sorafenib (*31*), sunitinib (*32*), pazopanib (*33*), and axitinib (*34*).

Similarities between two otherwise unrelated familial syndromes, von Hippel–Lindau, resulting from mutations in *VHL*, and tuberous sclerosis complex (TSC), resulting from mutations in the eponymic genes *TSC1* and *TSC2*, led us to hypothesize that mTORC1, which is regulated by the TSC1 and TSC2 proteins, may be implicated in renal

[1]Department of Developmental Biology, University of Texas Southwestern Medical Center, Dallas, TX 75390, USA. [2]Department of Internal Medicine, Oncology Division, University of Texas Southwestern Medical Center, Dallas, TX 75390, USA. [3]Simmons Comprehensive Cancer Center, University of Texas Southwestern Medical Center, Dallas, TX 75390, USA. [4]Illumina Cambridge Ltd., Chesterford Research Park, Little Chesterford, Essex CB10 1XL, UK. [5]Department of Biochemistry, University of Texas Southwestern Medical Center, Dallas, TX 75390, USA. [6]Department of Urology, University of Texas Southwestern Medical Center, Dallas, TX 75390, USA. [7]Department of Pathology, University of Texas Southwestern Medical Center, Dallas, TX 75390, USA.
*To whom correspondence should be addressed. E-mail: james.brugarolas@utsouthwestern.edu

Table 1. Patient demographics and characteristics of tumors implanted. Data in bold indicate tumorgraft lines giving rise to stable lines (TG ≥ 2). TG, tumorgraft; Mut, mutation (germline and somatic); wt, wild type; Sarc., sarcomatoid differentiation; Grade, Fuhrman nuclear grade; pT, pathologic T stage; pN, pathologic N stage; TG-0, histologically confirmed tumor in recipient mouse cohort; TG ≥ 2, histologically confirmed tumor passaged more than twice in mice; n/a, not applicable or assessed; Uni, unifocal; Multi, multifocal; M, male; F, female; Y, yes; N, no.

	T (ID)	Age (years)	Sex	*VHL*	Source	Histology	Sarc.	Grade	Focality	Size (cm)	pT	pN	TG-0	TG ≥ 2
1	114	69	M	Mut	Primary	Clear cell	Y	4	Uni	10.0	3	0	Y	N
2	**115**	**65**	**F**	**Mut**	**Primary**	**Clear cell**	**N**	**4**	**Uni**	**8.0**	**2**	**×**	**Y**	**Y**
3	116	66	M	Mut	Primary	Clear cell	Y	n/a	Uni	17.0	4	0	N	N
4	117	61	M	n/a	Primary	Papillary	N	3	Uni	4.0	1	×	N	N
5	118	65	F	Mut	Primary	Clear cell	N	2	Uni	2.5	1	×	N	N
6	119	79	F	n/a	Primary	Clear cell	N	3	Uni	5.7	1	×	N	N
7	120	62	M	n/a	Primary	Clear cell	N	1	Uni	2.9	1	×	N	N
8	**121**	**78**	**F**	**n/a**	**Primary**	**Papillary**	**N**	**2**	**Uni**	**3.0**	**1**	**×**	**Y**	**Y**
9	122	68	F	n/a	Primary	Chromophobe	N	3	Uni	25.0	3	0	N	N
10	123	56	M	n/a	Primary	Papillary	N	3	Multi	3.1	1	×	N	N
11	124	63	M	n/a	Primary	Clear cell	N	2	Uni	3.2	1	×	N	N
12	125	62	F	Mut	Primary	Clear cell	N	2	Uni	4.5	1	×	Y	N
13	126	53	M	Mut	Primary	Clear cell	N	2	Uni	4.5	1	×	N	N
14	**127**	**35**	**M**	**Mut**	**Primary**	Clear cell	**N**	**3**	**Uni**	**6.2**	**3**	**×**	**Y**	**Y**
15	128	71	M	Mut	Primary	Clear cell	N	3	Uni	4.0	1	×	N	N
16	129	67	M	n/a	Metastasis	Clear cell	N	n/a	n/a	4.0	n/a	n/a	N	N
17	130	61	F	Mut	Primary	Clear cell	N	2	Uni	6.0	3	×	N	N
18	131	49	F	Mut	Primary	Clear cell	N	2	Uni	3.0	1	0	Y	N
19	132	57	M	n/a	Primary	Papillary	N	3	Uni	7.9	2	0	N	N
20	133	58	F	Mut	Primary	Clear cell	N	2	Uni	7.2	3	0	N	N
21	134	59	F	n/a	Primary	Clear cell	N	2	Uni	1.1	1	×	N	N
22	135	63	M	n/a	Primary	Clear cell	N	1	Uni	2.9	1	×	N	N
23	136	73	F	wt	Primary	Clear cell	N	2	Uni	8.5	2	×	N	N
24	137	77	M	n/a	Primary	Papillary	N	3	Uni	2.2	1	×	Y	N
25	138	68	F	n/a	Primary	Chromophobe	N	2	Uni	5.4	1	×	N	N
26	139	66	M	n/a	Primary	Papillary	N	2	Uni	8.5	2	×	Y	N
27	140	52	M	n/a	Primary	Papillary	N	3	Multi	6.2	1	×	N	N
28	141	51	M	n/a	Primary	Chromophobe	N	3	Uni	5.7	1	×	N	N
29	**142**	**56**	**F**	**Mut**	**Primary**	**Clear cell**	**N**	**3**	**Uni**	**8.6**	**3**	**×**	**Y**	**Y**
30	**143**	**74**	**F**	**wt**	**Primary**	**Clear cell**	**Y**	**4**	**Uni**	**11.0**	**4**	**×**	**Y**	**Y**
31	**144**	**71**	**M**	**Mut**	**Primary**	**Clear cell**	**N**	**4**	**Uni**	**7.5**	**2**	**1**	**Y**	**Y***
32	145	55	F	Mut	Primary	Clear cell	N	2	Uni	7.0	1	×	Y	N
33	146	60	F	Mut	Primary	Clear cell	N	2	Uni	4.0	1	×	N	N
34	147	59	M	n/a	Primary	Liposarcoma	n/a	n/a	n/a	14.0	n/a	n/a	N	N
35	148	64	M	n/a	Primary	Papillary	N	2	Uni	6.5	1	×	N	N
36	149	56	M	wt	Primary	Clear cell	Y	4	Uni	11.5	3	0	N	N
37	150	50	F	Mut	Primary	Clear cell	N	3	Uni	6.7	3	×	Y	N
38	151	74	M	Mut	Primary	Clear cell	N	2	Uni	7.7	2	×	Y	N
39	**152**	**25**	**F**	**n/a**	**Metastasis**	**Papillary**	**N**	**n/a**	**n/a**	**4.5**	**n/a**	**n/a**	**Y**	**Y**
40	153	62	M	Mut	Primary	Clear cell	N	2	Uni	3.5	1	×	Y	N
41	154	62	M	n/a	Primary	Oncocytoma	N	n/a	n/a	4.0	n/a	n/a	N	N
42	155	64	M	Mut	Primary	Clear cell	Y	4	Uni	10.0	3	0	N	N
43	**156**	**65**	**F**	**n/a**	**Primary**	**Papillary**	**N**	**3**	**Uni**	**11.5**	**2**	**0**	**Y**	**Y**
44	157	72	F	Mut	Primary	Clear cell	N	2	Uni	5.2	1	×	N	N
45	**158**	**82**	**F**	**Mut**	**Primary**	**Clear cell**	**Y**	**3**	**Multi**	**12.7**	**3**	**×**	**Y**	**Y**

continued on next page

	T (ID)	Age (years)	Sex	*VHL*	Source	Histology	Sarc.	Grade	Focality	Size (cm)	pT	pN	TG-0	TG ≥ 2
46	159	24	M	n/a	Primary	Clear cell	N	2	Multi	3.0	1	×	N	N
47	160	62	M	Mut	Primary	Clear cell	N	2	Uni	4.2	1	×	N	N
48	161	36	M	Mut	Primary	Clear cell	N	2	Uni	8.4	2	×	Y	N
49	162	56	M	Mut	Primary	Clear cell	N	3	Uni	7.2	3	×	Y	N
50	163	52	M	Mut	Primary	Clear cell	Y	4	Uni	4.5	1	0	N	N
51	**164**	**75**	**M**	**wt**	**Primary**	**Clear cell**	**Y**	**4**	**Uni**	**11.3**	**4**	**×**	**Y**	**Y**
52	**165**	**42**	**M**	**Mut**	**Metastasis**	**Clear cell**	**N**	**3**	**n/a**	**1.3**	**n/a**	**n/a**	**Y**	**Y**
53	**166**	**56**	**M**	**Mut**	**Primary**	**Clear cell**	**Y**	**4**	**Uni**	**9.0**	**3**	**1**	**Y**	**Y***
54	167	74	M	n/a	Primary	Clear cell	N	3	Uni	4.0	1	×	N	N
55	**168**	**53**	**M**	**n/a**	**Primary**	**Unclassified**	**Y**	**4**	**Uni**	**8.0**	**3**	**1**	**Y**	**Y**
56	**169**	**52**	**M**	**n/a**	**Primary**	**Unclassified**	**N**	**4**	**Uni**	**5.5**	**4**	**1**	**Y**	**Y**
57	170	62	F	Mut	Primary	Clear cell	N	4	Uni	8.0	3	0	N	N
58	171	62	F	Mut	Primary	Clear cell	N	2	Uni	4.2	1	×	N	N
59	172	61	F	n/a	Primary	Cystic nephroma	N	n/a	n/a	10.7	n/a	n/a	N	N
60	173	50	M	Mut	Primary	Clear cell	N	3	Multi	12.0	3	×	Y	N
61	174	70	F	n/a	Primary	Oncocytoma	N	n/a	n/a	3.5	n/a	n/a	N	N
62	175	62	F	Mut	Primary	Clear cell	N	4	Uni	11.5	2	0	N	N
63	176	71	M	n/a	Primary	Papillary	N	3	Uni	11.5	3	1	N	N
64	177	56	F	n/a	Primary	Clear cell	N	2	Uni	3.2	1	×	Y	N
65	178	51	M	n/a	Primary	Papillary	N	2	Uni	5.5	1	×	Y	N
66	179	60	M	n/a	Primary	Clear cell	N	3	Uni	7.5	2	×	N	N
67	**180**	**56**	**M**	**Mut**	**Metastasis**	**Clear cell**	**N**	**n/a**	**n/a**	**3.5**	**n/a**	**n/a**	**Y**	**Y**
68	181	71	M	n/a	Primary	Clear cell	N	3	Uni	12.0	3	0	N	N
69	182	65	M	n/a	Primary	Clear cell	N	3	Uni	6.0	3	1	N	N
70	183	56	M	Mut	Primary	Clear cell	N	2	Uni	4.3	1	×	N	N
71	184	49	M	Mut	Primary	Clear cell	N	3	Uni	10.0	3	0	N	N
72	185	78	F	n/a	Primary	Oncocytoma	N	n/a	n/a	6.0	n/a	n/a	Y	N
73	186	51	M	n/a	Primary	Papillary	N	3	Uni	9.0	2	×	N	N
74	187	45	M	n/a	Primary	Unclassified	N	3	Multi	18.0	3	1	N	N
75	188	54	F	n/a	Primary	Clear cell	N	2	Uni	2.6	1	×	N	N
76	189	76	M	n/a	Primary	Oncocytoma	N	n/a	n/a	4.0	n/a	n/a	N	N
77	190	63	M	n/a	Primary	Papillary	N	3	Uni	7.5	2	×	N	N
78	191	83	M	Mut	Primary	Clear cell	N	3	Uni	9.6	3	×	Y	N
79	192	63	F	Mut	Primary	Clear cell	N	2	Uni	6.8	1	0	Y	N
80	193	70	M	Mut	Primary	Clear cell	N	3	Uni	12.0	2	0	N	N
81	194	56	F	Mut	Primary	Clear cell	N	3	Uni	4.5	3	×	N	N
82	195	71	F	Mut	Primary	Clear cell	N	3	Uni	5.3	3	×	N	N
83	196	57	F	n/a	Primary	Chromophobe	N	2	Uni	11.5	2	0	N	N
84	197	60	M	Mut	Primary	Clear cell	N	3	Uni	8.5	2	×	N	N
85	198	51	F	n/a	Primary	Clear cell	N	2	Uni	4.5	1	0	N	N
86	199	50	M	wt	Primary	Clear cell	N	3	Uni	13.0	3	0	Y	N
87	200	59	F	n/a	Primary	Oncocytoma	N	n/a	n/a	3.5	n/a	n/a	N	N
88	201	60	M	n/a	Primary	Clear cell	N	2	Multi	5.7	1	0	N	N
89	202	66	M	Mut	Primary	Clear cell	N	3	Uni	13.3	3	0	N	N
90	203	65	F	n/a	Primary	Clear cell	N	2	Uni	3.5	1	×	Y	N
91	204	61	F	wt	Primary	Clear cell	N	2	Uni	3.5	1	×	N	N
92	205	47	F	Mut	Primary	Clear cell	N	3	Uni	5.1	1	×	N	N
93	**206**	**72**	**M**	**n/a**	**Metastasis**	**Clear cell**	**N**	**n/a**	**n/a**	**1.1**	**n/a**	**n/a**	**Y**	**Y**
94	207	49	F	n/a	Primary	Angiomyolipoma	N	n/a	n/a	4.5	n/a	n/a	N	N

*Tumor noted to induce hypercalcemia in tumorgraft.

cancer (*35*). mTORC1 regulates cell growth and is constitutively activated in most ccRCCs (*36*–*39*). It is negatively regulated by a complex formed by TSC1 and TSC2, and somatically acquired *TSC1* mutations occur in ~5% of sporadic ccRCCs (*40*). How mTORC1 is activated in most ccRCC remains unknown, but mTORC1 is allosterically inhibited by rapamycin (sirolimus), and two sirolimus analogs, temsirolimus (*41*) and everolimus (*42*), have been approved by the FDA.

Herein, we report the development and validation of an RCC tumorgraft model for the evaluation of molecularly targeted therapies.

RESULTS

Establishment of tumorgrafts

Between September 2009 and January 2011, 94 tumors obtained from patients with kidney cancer were implanted in mice. Eligibility criteria were based on preoperative imaging studies and included tumors at least 5 cm in diameter, multifocal, bilateral or recurrent tumors, suspicion of invasion beyond the renal parenchyma, and regional or distant metastasis. In a few instances, samples were implanted from metastatic sites (Table 1). More than 90% of the tumors were RCCs and 75% were of clear-cell type. *VHL* mutations were detected in 87% of ccRCCs examined (Table 1). More than 50% of the RCCs were of high grade, and sarcomatoid elements were found in about 10%.

Tumor fragments from each site (2 to 3 mm in diameter) were implanted orthotopically, under the renal capsule, into five nonobese diabetic/severe combined immunodeficient (NOD/SCID) mice (Fig. 1A). To preserve tumor architecture and minimize confounding factors, we implanted samples without disaggregation or additives. Tumorgrafts were evident by magnetic resonance imaging (MRI) (Fig. 1B) and ultrasound (Fig. 1C), but palpation was typically sufficient for follow-up. When tumors reached ~10 mm in diameter, they were passaged. Passage occurred earlier if the mouse became sick or was getting old. At initial passage, tumor diameters ranged from about 4 to >10 mm (Fig. 1D). As determined histologically by examining recipient mice [tumorgraft cohort 0 (TGc0)], 37% of grafts formed viable tumors in mice (Table 1). The average latency period from the day of implantation until passage into the first cohort (TGc1) was highly variable, ranging from 1 to 8 months. The time was generally shorter for tumors with high nuclear grade or sarcomatoid elements and became shorter with sequential passage. At each passage, samples were fixed for histological analyses and, when sufficient material was available, samples were frozen for permanent storage [in dimethyl sulfoxide (DMSO)] and separately for molecular studies (Fig. 1A).

Orthotopic tumorgrafts resemble patient tumors histologically

Detailed analyses by a clinical pathologist specialized in genitourinary tumors (P.K.) showed that tumorgrafts retained not only the general morphology but also fine histological features of the corresponding tumors in patients. Even within a specific histological type, architectural

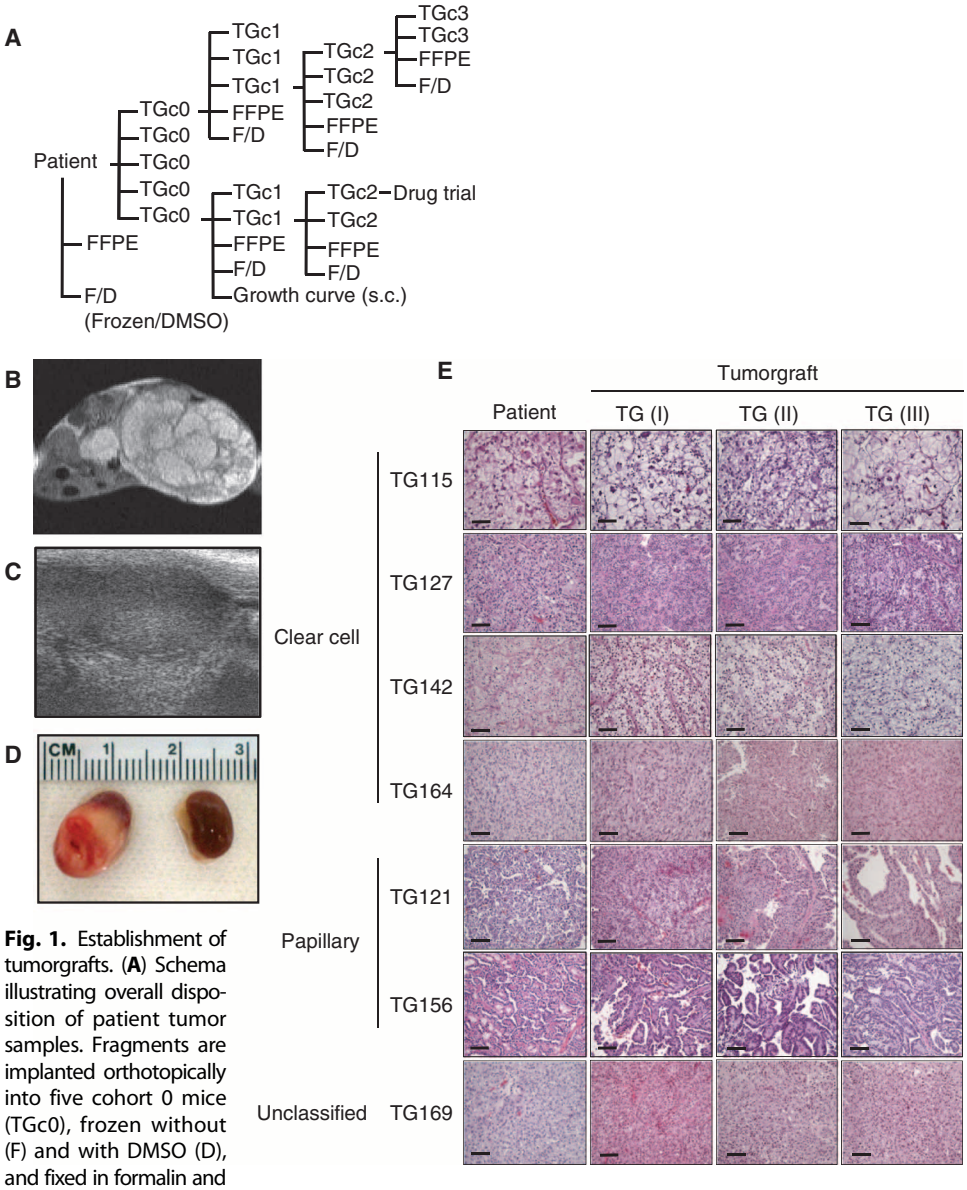

Fig. 1. Establishment of tumorgrafts. (**A**) Schema illustrating overall disposition of patient tumor samples. Fragments are implanted orthotopically into five cohort 0 mice (TGc0), frozen without (F) and with DMSO (D), and fixed in formalin and paraffin-embedded (FFPE). When tumorgrafts reach ~10 mm in diameter, they are passaged into cohort 1 mice (TGc1). After one or two passages, tumorgrafts are implanted for subcutaneous (s.c.) growth evaluation and, subsequently, for drug trials. Tumors from mice not passaged are processed and preserved. (**B**) MRI of orthotopic tumorgraft-bearing kidney in a mouse. (**C**) Renal ultrasound of tumorgraft. (**D**) Macroscopic images of engrafted tumor and contralateral kidney. (**E**) Representative H&E sections of patient tumor and corresponding tumorgrafts of increasing passages [TG(I), TG(II), and TG(III)]. Scale bars, 100 μm.

and cytological characteristics were preserved in the respective tumorgrafts (Fig. 1E). Overall, tumorgrafts maintained the growth pattern, as well as cystic components, the development of areas of necrosis and hemorrhage, sarcomatoid differentiation, cytological and nuclear features, Fuhrman nuclear grade, and the presence of inflammatory cells (table S1). In contrast, lymphocytic infiltrates were not preserved, which was expected because lymphocyte development is disrupted in NOD/SCID mice. Histological features were consistent despite serial passaging (Fig. 1E and table S1).

Predictors of stable tumor engraftment in mice

From 16 different patients, we were able to passage tumorgraft lines at least twice in mice (TGc $\geq$ 2), and these are referred to as stable lines. This sequential tumor growth in mice correlated with implantation from a metastatic site, sarcomatoid differentiation, high Fuhrman grade, pathologic tumor stage (a function of size and invasiveness), and the presence of regional lymph node or distant metastasis (Table 2). The same factors predicted engraftment when the analysis was limited to ccRCC (Table 2). The following did not predict for tumorgraft development in mice: histology, *VHL* mutation, focality, and tumor size. Notably, the engraftment rate of tumors implanted from metastases was considerably higher than those from primary tumors (80% versus 14%; $P = 0.0028$). Higher rates of engraftment were also observed with samples implanted from primary tumors of patients with distant metastases (60% versus 8%; $P = 0.0014$). These data suggested that the ability of tumors to grow serially in mice correlated with their ability to seed distant sites and metastasize.

Stable engraftment in mice is associated with poor survival in patients

Because stable engraftment correlated with metastases, we hypothesized that engraftment in mice may reflect the acquisition of metastatic potential by the primary tumor. As a result of short follow-up times and relatively small numbers of animals, the study was not powered to definitively address this question. Nevertheless, we asked whether a correlation existed between engraftment in mice and outcomes in patients presenting with localized disease. Patients whose tumors engrafted in mice had shorter survival times, possibly secondary to the development of metastases (Fig. 2). Similar results were observed when the analysis was limited to ccRCC (Fig. 2). Thus, stable engraftment in mice may predict poor outcomes in patients.

Tumorgrafts retain the gene expression pattern of the original tumor

To ascertain the extent to which RCC tumorgrafts maintained the characteristics of the tumor from which they were derived, we performed gene expression analyses. Because the recipient mice were immunodeficient, contributions from infiltrating lymphocytes to the global gene expression signature in tumors would be absent in tumorgrafts. In addition, because the stroma in the tumor is largely replaced by murine stroma (*43*), human stromal transcripts were likely underrepresented in tumorgrafts. To account for these differences, we subtracted transcripts up-regulated in tumors in comparison to tumorgrafts ($q < 0.05$ and fold change > 1.5-fold) (Fig. 3A). Pathway analyses on the subtracted probes showed that, as expected, they belonged largely to pathways implicated in immune-mediated processes such as antigen presentation, dendritic cell maturation, and natural killer (NK) signaling (Fig. 3A and table S2).

To determine whether tumorgrafts retained the gene expression pattern of the original tumor, we performed unsupervised hierarchical clustering analyses. Twenty-one of 29 (72%) tumorgrafts clustered together with the corresponding tumor (Fig. 3B). Clustering was maintained for cohort 7 and 8 tumorgrafts (Fig. 3B). Thus, the degree of similarity between most tumorgrafts and

Table 2. Predictors of stable tumor engraftment

	All histologies		ccRCC	
	Engrafted/ total	*P*	Engrafted/ total	*P*
RCC histology		0.15		
Clear cell	11/65			
Papillary	3/14			
Chromophobe	0/4			
Oncocytoma	0/5			
Unclassified	2/3			
VHL mutation (germline or somatic)				0.59
Mutant			8/42	
Wild type			2/6	
Tumor implanted from metastatic site	4/5	0.0028	3/4	0.014
Sarcomatoid differentiation	5/10	0.012	4/9	0.038
Fuhrman nuclear grade		0.0008		0.002
1	0/2		0/2	
2	1/32		0/26	
3	5/34		4/22	
4	7/13		5/11	
Focality		1.000		0.52
Unifocal	11/74		7/57	
Multifocal	1/7		1/4	
Size (cm)		0.58		0.30
≤4	4/27		3/19	
>4–7	3/28		1/19	
>7–10	5/21		4/16	
>10	4/18		3/11	
		0.0014		0.0026
Pathologic tumor stage		0.0014		0.0026
T1	1/37		0/28	
T2	3/15		2/9	
T3	5/25		4/21	
T4	3/4		2/3	
Pathologic lymph node stage		0.0077		0.016
N0	1/21		0/17	
N1	4/7		2/3	
Metastasis at presentation	6/10	0.0014	4/7	0.013

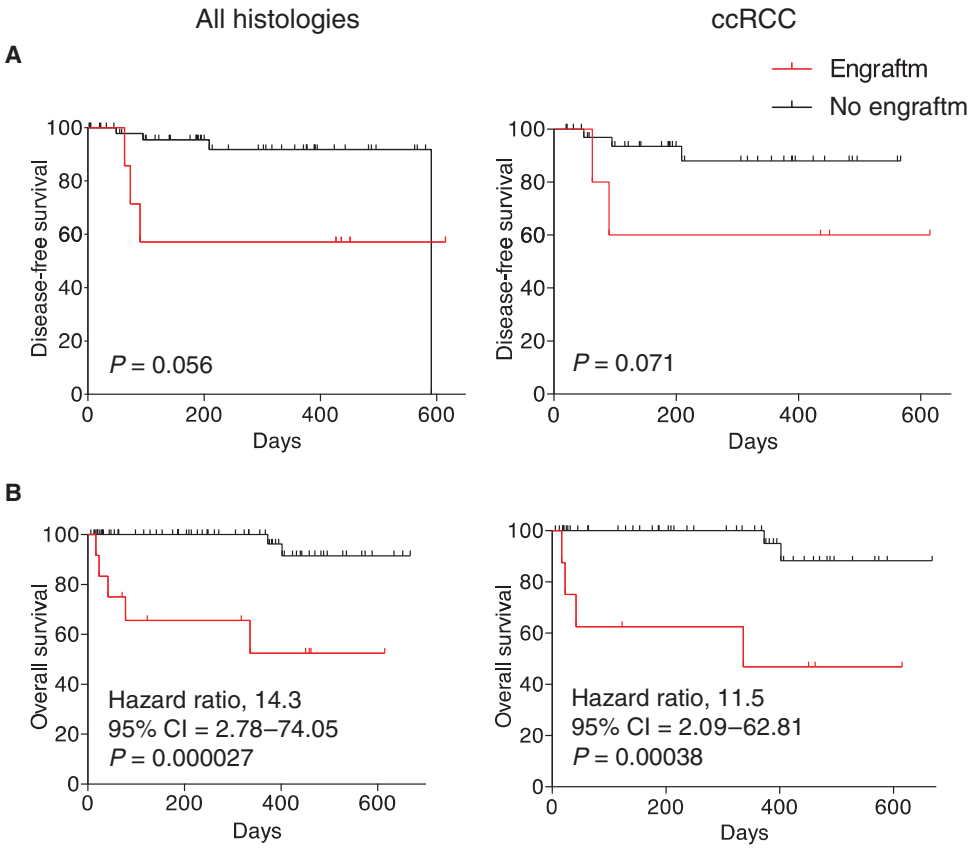

Fig. 2. Evaluation of patient outcomes as a function of stable engraftment of localized, primary tumors. (**A**) Kaplan-Meier analysis of disease-free survival for groups with and without stable engraftment for all histologies (left) or ccRCC (right). (**B**) Kaplan-Meier analysis of overall survival for groups with or without stable engraftment for all histologies (left) or ccRCC (right). Cross indicates censored data. CI, confidence interval.

the corresponding patient tumor was greater than between tumors from two different patients.

The approach we undertook also provided a means to separate gene expression signatures of tumor cells from those arising from nonneoplastic cells (Fig. 3C and tables S3 and S4). Not unexpectedly, reducing the contribution from nonneoplastic cells significantly affected the ranking of pathways deregulated in renal cancer and implicated some unexpected pathways, such as RAN signaling (table S4).

Tumorgrafts preserve the DNA copy number alterations of tumors

We evaluated DNA copy number alterations (CNAs) in tumorgrafts ranging from primary tumors in recipient mice (TGc0) to cohort 8 (TGc8). CNAs in tumorgrafts were characteristic of RCC, including chromosome 3p loss and less frequent deletions of chromosome 14 and 9p (*44*–*46*). Tumorgrafts largely retained the pattern of CNAs of the corresponding tumor irrespective of passage (Fig. 4A). To evaluate the extent to which CNAs in tumorgrafts resembled those in the tumor from which they were derived, we performed unsupervised hierarchical clustering analyses. Twenty of 27 (74%) tumorgrafts clustered with the corresponding tumor (Fig. 4B).

In one case, samples from tumorgraft lines were available for both a primary tumor and a corresponding metastasis. The metastasis had acquired some alterations that were not found in the primary tumor, including losses in chromosome 1 and 8 (Fig. 1C). CNAs in the tumorgrafts were indistinguishable from those in the metastasis and differed from the primary tumor (Fig. 1C). Thus, even within a single patient, tumorgrafts appear to retain the specific signature of the tumor or metastasis from which they were generated.

Point mutations and indels are preserved in tumorgrafts

We performed whole-genome (or exome) sequencing in seven tumors (*47*) and examined the preservation of mutations in tumorgrafts. A total of 134 somatically acquired point mutations or indels in protein-coding genes were examined in several tumorgraft cohorts [for specific mutations, refer to (*47*)]. Ninety-two percent of the mutations detected were retained in the tumorgrafts, and the number did not change significantly in later passages (Table 3). *VHL* mutations were uniformly retained in tumorgrafts in different cohorts [(*47*) and Table 4], which was expected, because *VHL* mutations occur early during ccRCC development (*48*).

Bidirectional Sanger sequencing of tumorgrafts was performed for 618 amplicons; we estimate that 247,200 base pairs of tumorgraft DNA were sequenced. Only one point mutation was confidently identified in a tumorgraft that was not detected in the primary tumor (Table 5). This mutation was in the *TSC1* gene, which we recently reported to be somatically inactivated in ccRCCs (*40*), and the corresponding patient's tumor had a different *TSC1* mutation. Very deep sequencing of two independent samples (~2 million reads per sample) showed that the mutation preexisted in the patient tumor at a frequency of 0.3% (table S5). Consistent with genome-wide studies in other tumor types (*49*), these data suggest that the acquisition of new mutations by RCC tumorgrafts is a rare event.

Development of paraneoplastic hypercalcemia in tumorgraft-bearing mice

We observed that some tumorgraft-bearing mice became ill. As tumorgrafts grew, the mice became progressively less active and more hunched, started losing weight, and eventually became moribund. The illness occurred only with specific tumorgraft lines (for example, TG144 and TG166), suggesting that the tumor was directly responsible. The symptoms were somewhat reminiscent of untreated hypercalcemia in humans, so we considered whether the tumorgrafts were inducing paraneoplastic hypercalcemia in mice. A review of the medical records of the corresponding patients showed that they had presented

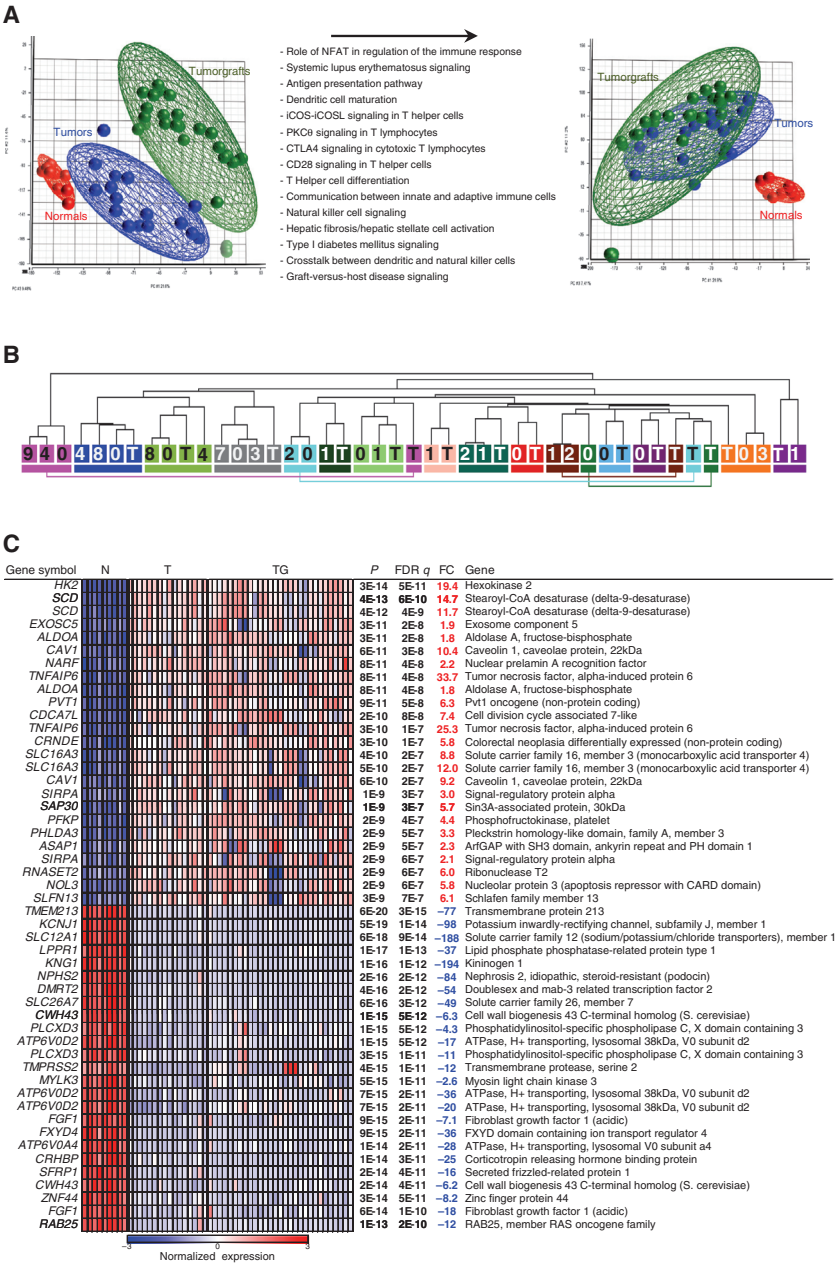

Fig. 3. Gene expression analyses of tumors and tumorgrafts. (**A**) Principal components analysis of tumor, paired normal renal cortex (for a subset of tumors), and tumorgraft samples before and after subtraction of genes differentially up-regulated in tumors (compared to tumorgrafts). List of top Ingenuity Pathways corresponding to transcripts up-regulated in tumors over tumorgrafts with a FDR $q < 0.05$ and a fold change greater than 1.5. (**B**) Unsupervised hierarchical clustering of samples according to gene expression pattern after subtraction. Each tumor/tumorgraft clade is color-coded and includes patient tumor sample (T) and the corresponding tumorgrafts (numbers reflect mouse tumorgraft cohort). (**C**) Heatmap of tumor-specific gene expression changes after subtraction of immune/stromal signature, including the top 25 up- and down-regulated genes in tumors compared to adjacent normal parenchyma (ranked by q value). N, normal; T, tumor; TG, tumorgraft; FDR q, false discovery rate–corrected P value; FC, fold change.

with elevated calcium concentrations and that the hypercalcemia resolved after tumor resection. To determine whether TG144 and TG166 tumorgraft-bearing mice similarly developed paraneoplastic hypercalcemia, we measured calcium levels. Whereas in control tumorgraft-bearing mice serum calcium levels were within the normal range (8.5 to 10.5 mg/dl), calcium levels reached >15 mg/dl in both TG144 and TG166 mice (Fig. 5). Thus, as indicated by their hypercalcemia, paraneoplastic syndrome may develop in tumorgraft-bearing mice.

Mimicking sunitinib and sirolimus exposures of RCC patients in NOD/SCID mice

The most critical aspect of the evaluation of a tumor model is whether it reproduces the drug responsiveness of tumors in patients. To determine whether RCC tumorgrafts retained the sensitivity of RCC in the clinic, we tested their sensitivity to an inhibitor of angiogenesis, sunitinib, and an mTORC1 inhibitor, sirolimus. We used sirolimus instead of temsirolimus, because temsirolimus is largely a sirolimus prodrug; in humans, after temsirolimus administration, 75% of circulating drug is sirolimus (*50*, *51*). We also previously reported the treatment of an RCC patient with sirolimus (before temsirolimus became commercially available) (*52*). As a control, we used a small-molecule kinase inhibitor that had been tested against RCC and was inactive, the epidermal growth factor receptor (EGFR) kinase inhibitor erlotinib, which is approved for non–small cell lung cancer (NSCLC) treatment. A randomized phase 2 trial of erlotinib in combination with bevacizumab failed to show improved outcomes in comparison to bevacizumab alone in patients with ccRCC (*53*).

Because the results of drug trials can be affected by differences in drug metabolism across species (*7*), we performed pharmacokinetic (PK) sudies in mice to identify a regimen that mimicked human exposures. We sought to balance sustained therapeutic levels (above the C_{min} in humans) without excessive peak (C_{max}) and total exposures (AUC_{last}). Because differences may exist in drug metabolism across mouse strains, NOD/SCID mice were used.

Sirolimus, at 0.5 mg/kg given intraperitoneally every 48 hours, resulted in trough levels within the therapeutic range in humans (5 to 15 ng/ml) (*54*, *55*). However, peak and overall exposures were two- to threefold higher than in humans (Table 6).

Sunitinib is metabolized to desethyl sunitinib, which is active, and PK studies were performed to evaluate both sunitinib and its metabolite. Whereas on day 1 the metabolite represented 13% of the total circulating drug in humans, it made up 38% in mice (Table 6). The half-life of sunitinib was much shorter in mice, and mice were treated every 12 hours. The administration of sunitinib (10 mg/kg) by gavage every 12 hours resulted in peak exposures that were slightly higher than in humans and overall exposures of the parent compound and metabolite that were within the range of exposures between day 1 and day 28 in humans (Table 6). Although sunitinib builds up in humans over time, troughs in mice are likely to be lower

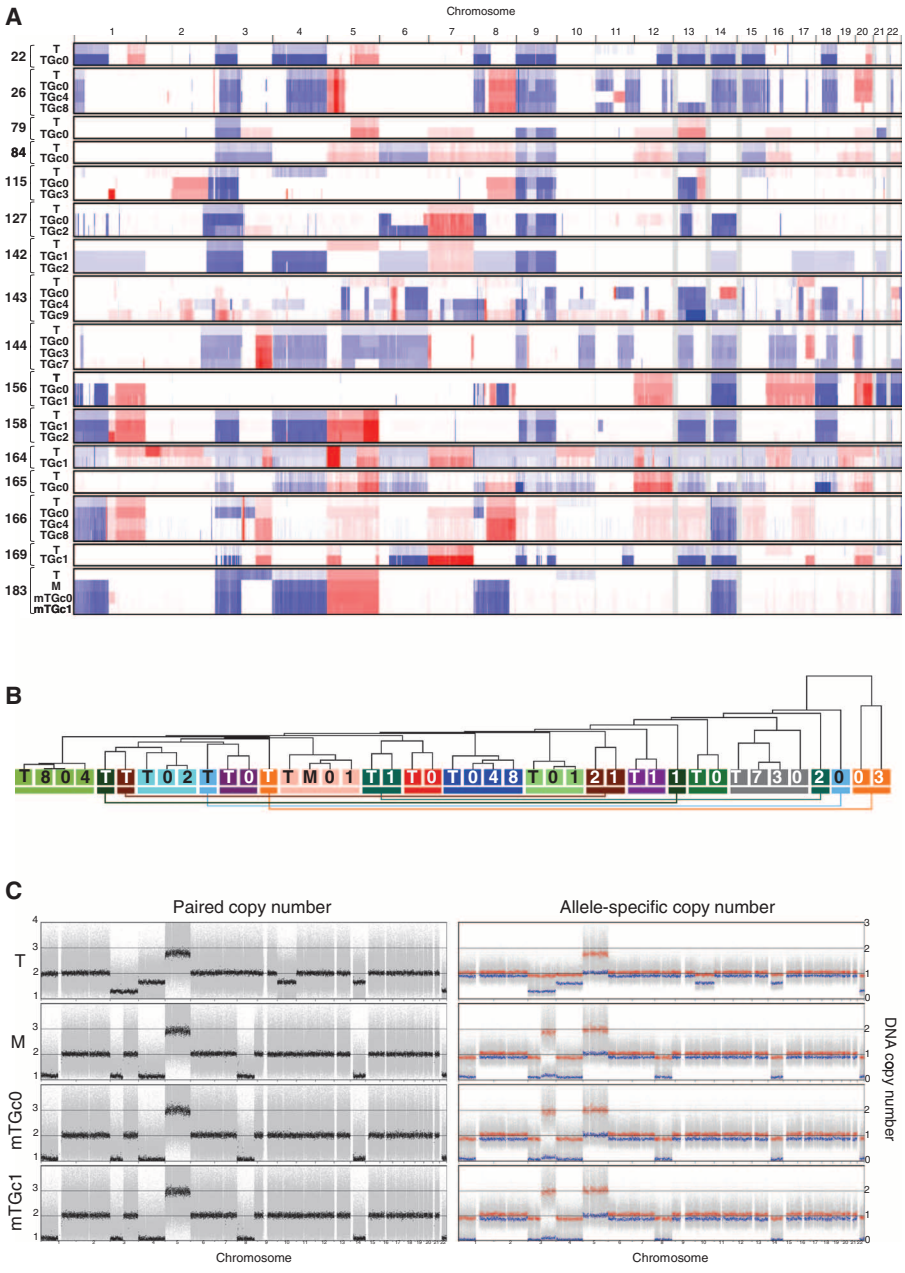

Fig. 4. DNA CNAs in tumors and tumorgrafts. (**A**) Representation of DNA copy numbers in patient tumors (T) and corresponding tumorgrafts from the indicated cohorts. Red, amplifications; blue, deletions. (**B**) Unsupervised hierarchical clustering of samples according to paired DNA copy number analyses. Each tumor/tumorgraft clade is color-coded and includes patient tumors (T) or metastasis (M) and corresponding tumorgrafts (numbers, which reflect cohort). (**C**) Paired copy number and allele-specific copy number analyses of a patient tumor (T), metastasis (M), and metastasis-derived tumorgrafts in the recipient mouse (mTGc0) and cohort 1 (mTGc1).

than in humans. Nevertheless, given the every 12-hour dosing, and the overall drug exposures, we considered this acceptable.

In humans, erlotinib is metabolized to *O*-desmethyl-erlotinib, which is active. The ratios of parent compound to metabolite were similar in humans and mice (Table 6). Whereas the half-life of erlotinib in humans is 24 hours (*56*), it was 3 hours in mice, and we treated mice every 12 hours. Because erlotinib was used as a negative control, it was preferable to err on the side of overdosing. Erlotinib at 12.5 mg/kg by gavage every 12 hours resulted in trough concentrations within the human range (*56*, *57*), although this resulted in higher peak and overall exposures (Table 6).

Tumorgrafts reproduce the drug responsiveness of RCC

The use of orthotopic tumorgrafts to study drug responsiveness is hampered by the need for frequent imaging to monitor tumor growth during drug trials. Because measurements were significantly easier for subcutaneous tumors, we evaluated the growth of orthotopically growing tumorgrafts in the subcutaneous space. Only ~65% of the tumorgraft lines growing orthotopically grew subcutaneously within a manageable timeframe. Despite the heterotopic location, RCC in humans sometimes metastasizes to the subcutaneous space and the histological characteristics were preserved (Fig. 6A). In addition, as determined in one tumorgraft line (TG164), drug effects did not differ whether the tumor was implanted subcutaneously or orthotopically, and we saw similar antitumor responses in earlier- and later-passage tumors (fig. S1).

Eight ccRCC tumorgraft lines that grew subcutaneously were evaluated in drug trials (Fig. 6A). For each trial, ~20 mice were implanted with ~64 mm^3 tumor fragments, and 2 to 4 weeks after implantation, tumor volume measurements begun. Tumor growth rates varied considerably among the eight tumorgraft lines, and drug administration started when average tumor size reached about 250 to 300 mm^3. To avoid biases from excessively weighting any particular dimension, we calculated tumor volumes according to the formula $l \times w \times h$, where l is maximal length, w is maximal width perpendicular to l, and h is maximal height. Tumorgraft-bearing mice of similar characteristics (tumor volume, tumor growth rate, and mouse weight) were distributed evenly across treatment arms. Arms were kept balanced, and statistical analyses at the completion of drug trials showed no biases at the start.

For each drug trial, three to five mice were allocated to one of four treatment groups: sirolimus, sunitinib, erlotinib, and vehicle. Drug trials were carried out for ~28 days. During the trial, tumor measurements were taken twice weekly. Mice were weighed weekly, and drug administration was adjusted accordingly.

A total of 122 mice, from eight different tumorgraft lines, were evaluated in drug trials (Fig. 6B; see also fig. S2). Using ccRCC vehicle-treated mice as a reference, erlotinib treatment had no statistically significant effect on tumorgraft growth (Fig. 6B). However, the same erlotinib

Table 3. Mutations retained in tumorgraft cohorts. n/a, not assessed; TG, tumorgrafts of increasing passages.

ID	No. of mutations evaluated	Retained mutations		
		TG(I)	TG(II)	TG(III)
TG22	48	45	n/a	n/a
TG144	22	20	20	19
TG166	21	21	21	21
TG180	13	13	13	n/a
TG164	12	11	11	n/a
TG142	11	8	8	n/a
TG127	7	5	5	n/a
Total	134	123 (92%)	78 (91%)	40 (93%)
Overall			241/263 (92%)	

Table 4. *VHL* mutations in patient tumors and tumorgrafts. n/a, not assessed; TG, tumorgrafts of increasing passages.

ID	*VHL* mutation (tumor)	Retained mutations		
		TG(I)	TG(II)	TG(III)
TG22	c.472C>G,p.L158V	+	n/a	n/a
TG127	c.232_233delAA	+	+	n/a
TG142	c.525_533delCAGGAGACT	+	+	n/a
TG144	c.506T>C,p.L169P	+	+	+
TG166	c.224_226delTCT	+	+	+
TG183	c.414_421delATCTCTCA	+	+	n/a

regimen had profound effects on a NSCLC cell line–derived xenograft used as a control (Fig. 6C). In contrast, ccRCC tumorgraft growth was substantially inhibited by treatment with sunitinib ($P < 0.0001$) (Fig. 6, B and D). Likewise, sirolimus inhibited tumorgraft growth ($P < 0.0001$) (Fig. 6, B and D).

Together, these data show that tumorgraft responses to drugs reproduce the sensitivity to sunitinib and (tem)sirolimus of RCC observed in the clinic.

Pharmacodynamic studies in tumorgrafts show mTORC1 pathway inhibition

Next we evaluated the effects of sirolimus and sunitinib on mTORC1 pathway activity in tumor cells. For this analysis, we used an antibody that recognizes phospho-S6$^{240/244}$ (p-S6$^{240/244}$), a faithful marker of mTORC1 activity (*58*). p-S6$^{240/244}$ immunohistochemistry was evaluated by a clinical pathologist (P.K.) who was blinded to the treatment allocation. Scores were determined by both signal intensity and the percentage of positive cells. A decrease in p-S6$^{240/244}$ was observed in sirolimus-treated tumorgrafts ($P < 0.0001$; see also Fig. 6E). A more modest, but significant, reduction in p-S6$^{240/244}$ was also observed after sunitinib treatment ($P = 0.021$). By contrast, erlotinib had no effect on p-S6$^{240/244}$ ($P = 0.62$).

Table 5. Point mutations or indels in tumorgrafts but not in patient tumors.

Total amplicons sequenced in tumorgrafts	618
Average number of base pairs per amplicon	400
Approximate number of base pairs sequenced	247,200
Mutations in tumorgrafts but not in patient tumors	1*

*Mutation detected in corresponding tumor by very deep sequencing.

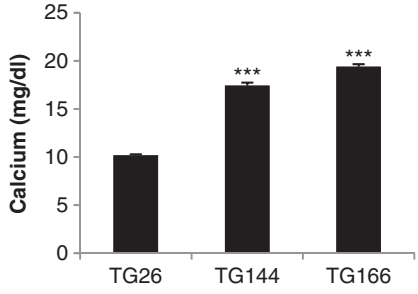

Fig. 5. Calcium levels in tumorgraft-bearing mice. Serum calcium concentrations in mice implanted with tumors from patients with paraneoplastic hypercalcemia, TG144 ($n = 3$) and TG166 ($n = 3$), compared to tumorgraft-bearing mice from a patient without paraneoplastic hypercalcemia (TG26; $n = 5$). Data are means ± SE; ***$P < 0.001$.

Dovitinib inhibits tumorgraft growth

Finally, we used our model to evaluate an investigational agent, dovitinib. Dovitinib is a highly potent inhibitor of VEGFR1, VEGFR2, VEGFR3, PDGFRβ, and FGFR1, FGFR2, and FGFR3 (fibroblast growth factor receptors 1, 2, and 3) (*59*) that is being evaluated in clinical trials, but its effectiveness against RCC is presently unknown. PK studies indicated that 30 mg/kg daily by gavage resulted in peak and overall exposures in mice within the range reported in humans (Table 6).

Clinical trials were conducted comparing dovitinib to sunitinib and sirolimus in four ccRCC tumorgraft lines, including a ccRCC tumorgraft line that we had not previously evaluated (TG206). Dovitinib markedly suppressed ccRCC tumorgraft growth (Fig. 7, A and B, and fig. S3), resulting in a greater inhibition of tumor growth than both sunitinib and sirolimus (Fig. 7, A to C). We also evaluated a papillary RCC tumorgraft line (TG121), in which dovitinib was also very active (fig. S3). In addition, dovitinib inhibited the development of paraneoplastic hypercalcemia in mice (Fig. 7D). Finally, as indicated by changes in body weight, dovitinib was not particularly detrimental in most mice (fig. S4). Overall, these results show that dovitinib was more effective against RCC tumorgrafts than sunitinib or sirolimus and that it is reasonably well tolerated.

DISCUSSION

RCC tumorgrafts in the mouse kidney reproduced the histology, gene expression, molecular genetics, and treatment responsiveness of RCC in patients. Our results in this study with FDA-approved drugs establish

Table 6. Pharmacokinetic analysis of drug regimens in mice with reference to human studies. Pharmacokinetic (PK) parameters (mean ± SE) based on noncompartmental analysis using WinNonlin (Pharsight Corp.). IP, intraperitoneal; IV, intravenous; PO, orally; G, gavage; qwk, weekly; qd, daily.

Drug	Species	Dose	Route	Schedule	PK data at	Analyte	AUC_{last} (ng h/ml)	C_{max} (ng/ml)	T_{max} (hours)	Terminal $t_{1/2}$ (hours)	C_{min} (ng/ml)	Reference
Sirolimus	**Mouse**	**0.5 mg/kg**	**IP**	**q48h**	**48 h**	**Sirolimus**	**4,276 ± 329**	**983 ± 98**	**1**	**13.6**	**14.9 ± 2.0**	
Temsirolimus	Human	25 mg	IV	qwk	D7 or D28	Temsirolimus	1,580 ± 270	595 ± 102	0.5	12.8		(*50*)*
						Sirolimus	3,810 ± 2,210	66 ± 35	1	48.8		
						Sum	5,860 ± 2,340					
Everolimus	Human	10 mg	PO	qd		Everolimus	514 ± 231	61 ± 17			13.2 ± 7.2	(*55*)*
Sunitinib malate	**Mouse**	**10 mg/kg**	**G**	**q12h**	**12 h (D1)**	**Sunitinib**	**449.8 ± 41.1**	**108.5 ± 5.5**	**2**	**2**	**4.2 ± 0.1**	
						Desethyl sunitinib	**174.4 ± 24.0**	**37.8 ± 0.2**	**2**	**2.6**	**3.0 ± 0.1**	
						Sum	**624.2**				**7.2**	
Sunitinib malate	Human	50 mg	PO	qd (D1–28)	24 h (D1)	Sunitinib	420 ± 210	27.7 ± 14.1	5			(*68*)*
						Desethyl sunitinib	63.6 ± 33.7	4.1 ± 2.2	5			
						Sum	483.6					
Sunitinib malate	Human	50 mg	PO	qd (D1–28)	24 h (D28)	Sunitinib	1,296 ± 609	72.2 ± 31.0	8.5		44.0 ± 26.0	(*68*)*
						Desethyl sunitinib	592 ± 391	33.7 ± 24.6	6.5		18.8 ± 8.5	
						Sum	1,888				62.8	
Erlotinib	**Mouse**	**12.5 mg/kg**	**G**	**q12h**	**12 h (D1)**	**Erlotinib**	**27,042 ± 2,569**	**3,513 ± 271**	**3**	**3.1**	**521 ± 169**	
						Desmethyl erlotinib	**3,970 ± 330**	**526 ± 77**	**3**	**2.5**	**50 ± 23**	
Erlotinib	Human	150 mg	PO	qd	24 h (D1)	Erlotinib	11,860 ± 5,010	872 ± 399	3		385 ± 213	(*57*)*
						Desmethyl erlotinib	835 ± 479	68 ± 45	3.6		25 ± 18	
Erlotinib	Human	150 mg	PO	qd	24 h (D28)	Erlotinib	43,760 ± 22,560	2,528 ± 1,187		24.2	1,473 ± 877	(*56*)*
Dovitinib	**Mouse**	**30 mg/kg**	**G**	**qd**	**24 h (D1)**	**Dovitinib**	**6,078 ± 710**	**373 ± 14.6**	**6**	**5.4**	**41.2 ± 9.3**	
Dovitinib	Human	500 mg	PO	5 d on/ 2 d off	24 h (D1)	Dovitinib	2,200 – 8,251	180 – 487				(*69*)*
Dovitinib	Human	500 mg	PO	qd	24 h (D1)	Dovitinib	3,734 ± 2,115	223 ± 128				(*70*)*
					(D15)	Dovitinib	4,340 ± 3,775	267 ± 178		21		

*Mean ± SD.

a proof of principle for the evaluation of molecularly targeted therapies for renal cancer in mice. We used this platform to evaluate an agent in clinical development, dovitinib, which shows remarkable activity against RCC.

Tumorgrafts reproduced not only the histology of the patient tumor but also finer characteristics such as tumor architecture as well as cytological and nuclear features. In unsupervised hierarchical clustering analyses of gene expression or DNA copy numbers, about 70% of tumorgrafts clustered together with the corresponding tumors from patients. There were greater similarities between tumorgrafts and their corresponding tumors than between tumors from different patients. Even within a single patient, DNA copy number analyses showed that a metastasis-derived tumorgraft was more similar to the metastasis than the metastasis was to the primary tumor. Notably, tumorgrafts preserved 92% of the somatically acquired protein-coding gene mutations of the patient tumors. In addition, these studies did not reveal any point mutations or indels in the tumorgraft that could not be found in the original patient tumor. Overall, our results show that tumorgrafts in mice are faithful models of the corresponding tumors in humans.

RCC tumorgrafts retained the drug sensitivity of RCC in the clinic. We performed large, controlled experiments with clinically relevant drug regimens, giving exposures comparable to those in humans. The

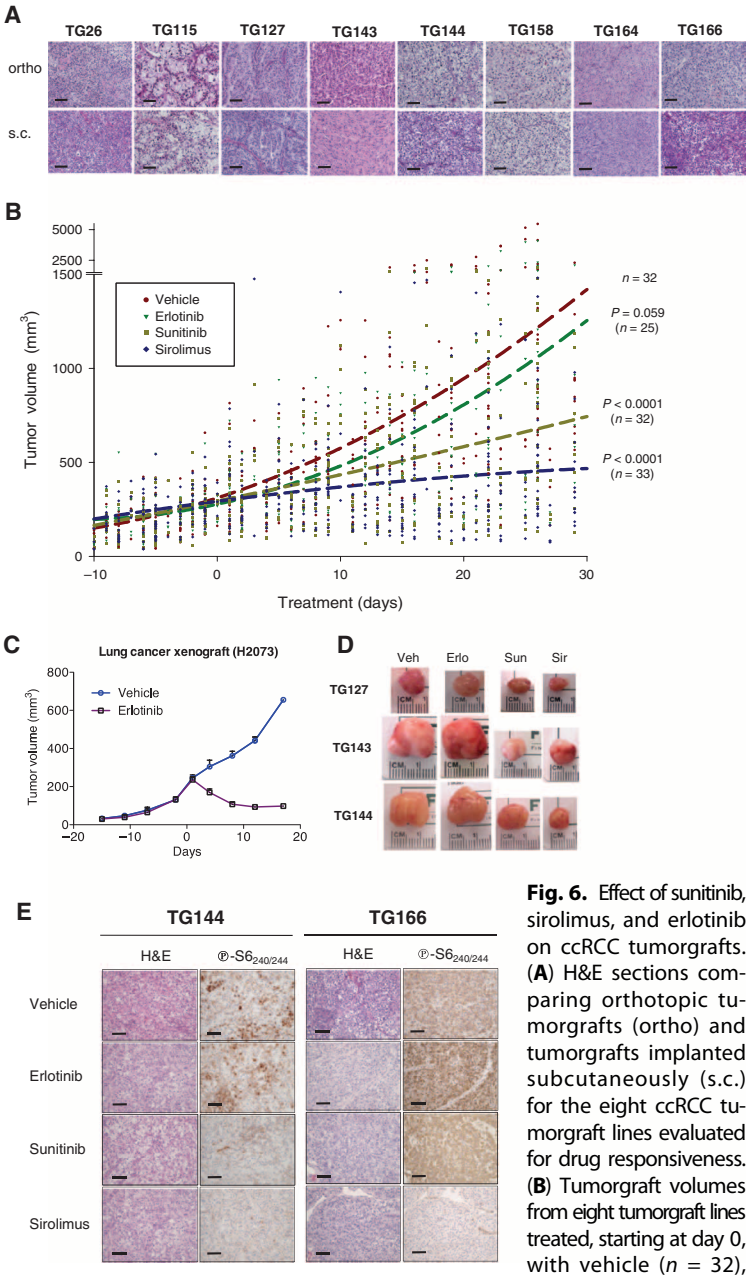

Fig. 6. Effect of sunitinib, sirolimus, and erlotinib on ccRCC tumorgrafts. (**A**) H&E sections comparing orthotopic tumorgrafts (ortho) and tumorgrafts implanted subcutaneously (s.c.) for the eight ccRCC tumorgraft lines evaluated for drug responsiveness. (**B**) Tumorgraft volumes from eight tumorgraft lines treated, starting at day 0, with vehicle (n = 32), erlotinib (n = 25), sunitinib (n = 32), and sirolimus (n = 33). Graph includes 1482 volume measurements (vehicle, n = 385; erlotinib, n = 304; sunitinib, n = 380; and sirolimus, n = 413). Trend lines were generated with a second-order polynomial quadratic regression analysis. P values in comparison to vehicle control were determined with a linear mixed model. (**C**) Tumor volumes of lung adenocarcinoma cell line–derived xenografts from mice treated with erlotinib (n = 3) or vehicle (n = 3). Data are means ± SE. (**D**) Representative macroscopic tumorgraft images from several tumors from different lines at the end of the trial. (**E**) Immunohistochemistry of tumorgrafts from mice treated as indicated and evaluated for the mTORC1 pathway effector marker phospho-S6. Scale bars, 100 μm.

tumorgrafts retained the sensitivities to sunitinib and (tem)sirolimus observed in the clinic, and failed to respond to the control, erlotinib. These data establish the validity of tumorgrafts as a model for the evaluation of targeted therapies for this cancer and potentially for others.

Two studies have reported similar results (*60*, *61*). They evaluated two ccRCC tumorgraft lines, and, in one study, a single mouse from each line was treated per condition (*61*). In the other study, tumorgraft growth was inhibited by sorafenib (*60*), although it is not clear whether the sorafenib regimen was clinically relevant, and the specificity of the response could not be ascertained because of a lack of a control drug. In addition, the admixing of tumorgraft tissue with Matrigel raises the possibility that sorafenib inhibition may have resulted, at least in part, from inhibition of the effects of ectopic growth factors in the extract. Nevertheless, these results are consistent with our data.

Dovitinib, an investigational agent in clinical development, more potently inhibited RCC tumorgraft growth than did sunitinib and sirolimus. Our results in our validated tumorgraft model lead us to predict that dovitinib will similarly be effective against renal cancer in humans. These data support the evaluation of dovitinib in randomized clinical trials of RCC patients in comparison to sunitinib and temsirolimus.

Tumorgraft engraftment may reflect metastatic potential. We saw a correlation between stable engraftment in mice and poor survival. We hypothesize that tumorgraft growth in mice reflects the acquisition by the tumor of a capability to thrive at other sites, which is characteristic of metastases. Consistent with this notion, samples implanted from metastatic sites engrafted at higher frequencies than those from primary tumors. Thus, tumorgrafts may help dissect biological determinants of metastases.

Tumorgraft features were preserved despite serial passage in mice. In addition, whereas divergence is expected with passage in mice over time, late-passage tumorgrafts did not appear to accumulate mutations. Finally, neither passage nor subcutaneous implantation seemingly affected tumorgraft responsiveness to drugs. Whereas the engraftment frequency in mice was 37%, stable tumorgraft lines were obtained in about half (17%). Several factors may account for the low rate of stable engraftment including residual NK function in NOD/SCID mice and tumorgraft loss because of infiltration by lymphoma cells arising spontaneously in aged NOD/SCID mice.

Inasmuch as the only cellular compartment that regenerates in tumorgrafts over the long term is the neoplastic compartment (*43*), tumorgrafts may contain nearly pure populations of human tumor cells, and this may have important applications. Tumorgrafts are useful for accurately determining mutant allele frequencies in tumors (*47*), and, given the mutation heterogeneity in RCC (*48*, *62*), they may aid in the identification of driver mutations. In addition, tumorgrafts provide a means to separate gene expression signatures arising from the tumor from those contributed by nonmalignant immune and stromal cells. The immune cell signature could be applied to shed light into an important but very difficult clinical problem, the elucidation of determinants of tumor responsiveness to high-dose IL-2.

Tumorgrafts have many other applications. Inasmuch as they retain the mutations of patient tumors and preserve their drug responsiveness, they can be used to determine whether targeting a specific pathway disrupted by mutation results in antitumor effects. Tumorgrafts can be used to determine whether a target was successfully inhibited in the tumor, which is a challenge in patients. They can help to prioritize drug combinations and to dissect difficult problems such as how resistance to antiangiogenic agents develops.

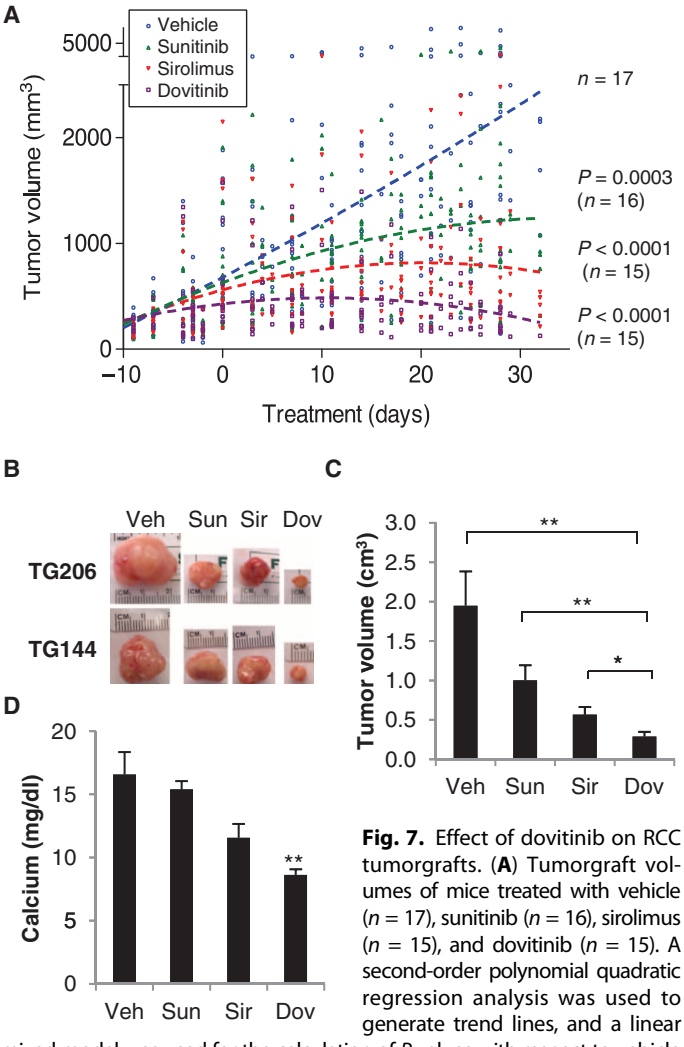

Fig. 7. Effect of dovitinib on RCC tumorgrafts. (**A**) Tumorgraft volumes of mice treated with vehicle ($n = 17$), sunitinib ($n = 16$), sirolimus ($n = 15$), and dovitinib ($n = 15$). A second-order polynomial quadratic regression analysis was used to generate trend lines, and a linear mixed model was used for the calculation of P values with respect to vehicle control. (**B**) Macroscopic tumorgraft images from several tumors at the end of trial. (**C**) Tumorgraft volumes at the end of drug trial. (**D**) Serum calcium concentrations of TG144 at the end of the trial ($n = 3$ to 4 per treatment arm). Data are means ± SE. *$P < 0.05$; **$P < 0.01$.

They provide an experimental system in which to investigate poorly understood aspects of tumor biology such as paraneoplastic syndromes and cancer-induced cachexia. The exploitation of differences across species may render tumorgraft-bearing mice useful for the identification of tumor markers. In addition, tumorgrafts can be used to study unusual forms of RCC; recently, we derived a tumorgraft line from a papillary RCC of a patient with a de novo germline mutation in fumarate hydratase (*63*). Finally, tumorgrafts may be useful to evaluate new imaging modalities and to assess, for instance, the effects of HIF on metabolism (*64*).

In summary, this study establishes a proof of concept for the development and application of RCC tumorgrafts for the evaluation of molecularly targeted therapies. We propose that the routine incorporation of such models into the development of molecularly targeted drugs could advance preclinical drug evaluation programs and improve oncology drug development.

MATERIALS AND METHODS

Regulatory

Patients enrolled in the study provided written consent allowing the use of discarded surgical samples for research purposes and genetic studies according to an Institutional Review Board–approved protocol. Tumorgraft studies were based on a protocol approved by the University of Texas Southwestern Medical Center Institutional Animal Care and Use Committee.

Nomenclature and annotation

Patient tumor samples were designated as T, followed by the ID. Tumors growing in mice are referred to as tumorgrafts (designated as TG, followed by the ID). Tumorgrafts arising in the recipient mouse are designated as TGc0 (TG cohort 0). Subsequent tumorgraft passages are designated by TG followed by the cohort number (for example, TGc1, TGc2, etc.). TG followed by a roman numeral in brackets indicates a specific sequence of tumorgrafts without specifying the cohort, for example, TG(I), TG(II), TG(III), where (I) precedes (II) and so on. T22, T26, T79, and T84 (and the respective TGs) correspond to ccRCCs obtained before the series described in Table 1.

Tumor samples (pT) were annotated on the basis of the American Joint Committee on Cancer tumor-node-metastasis (TNM) classification and the edition corresponding to the date of surgery. However, based on the 7th edition, all lymph node metastases are referred to as pN1.

Tumorgraft sample processing and implantation

Eligibility criteria were based on preoperative imaging studies and included renal tumor samples greater than 5 cm, multiple, bilateral or recurrent tumors, suspicion of invasion, lymphadenopathy, and distant metastasis. Any of these criteria were sufficient for inclusion. Patients were excluded if they were known to be positive for hepatitis B virus, hepatitis C virus, or HIV. Samples were collected, placed on ice, and typically processed within 3 hours. They were transferred to a sterile dish with phosphate-buffered saline and cut into 8 to 27 mm^3 fragments.

Typically, 4- to 6-week-old male or female NOD/SCID mice were used for implantation. Mice were anesthetized by inhalation with an isoflurane vaporizer, and 0.0015 mg of buprenorphine was administered by intraperitoneal injection immediately after surgery, while the mice were still anesthetized, and within 24 hours after surgery. Mice were placed on a warming pad, fur was shaved, and the area was sterilized with Betadine. A transverse incision was made posteriorly over the mid lumbar spine, and the skin was bluntly dissected. A smaller ~1 cm incision in the same direction was made of the body wall over the left flank, and the kidney was exteriorized by gently applying pressure. A 2-mm longitudinal incision was made in the dorsal aspect of the kidney with spring-loaded scissors. A pocket was carefully created underneath, avoiding damage to the parenchyma, which would otherwise bleed, and two to three samples were gently pushed inside. The kidney was eased back into the retroperitoneum, the body wall was sutured, and the skin was stapled.

Additional fragments were frozen at −80°C or placed in 10% DMSO in Hanks' balanced salt solution (HBSS), frozen at −80°C, and subsequently transferred within 7 days to liquid nitrogen. In addition, a sample was fixed in 10% buffered formalin acetate, paraffin-embedded, and stained with hematoxylin and eosin (H&E). Light microscopic evaluation of tissue sections was performed by a urological pathologist (W.K.

or P.K.). Images were obtained with a Nikon Eclipse 80i microscope and NIS-Elements D 3.10 camera.

Mice were evaluated for tumor growth by physical exam typically twice weekly. When tumors reached ~10 mm in diameter, or mice became ill, they were anesthetized with isoflurane and exsanguinated by cardiac puncture, and tumors were processed as above and serially transplanted into subsequent cohorts of NOD/SCID mice.

Serum calcium was measured at the University of Texas Southwestern Mouse Metabolic Phenotyping Core with a Vitros 250 Chemistry System (Johnson and Johnson).

Tissue processing for genomic studies

Flash-frozen samples preserved at −80°C were processed while on dry ice. Tumor content and sample quality was determined through pathological analyses (W.K.) of flanking sections oriented with pathology dyes (StatLab Medical Products). These were fixed in formalin and paraffin-embedded. Tumor and tumorgraft samples were carefully selected to ensure >70% tumor cellularity and the absence of necrosis or hemorrhage. Normal benign renal cortex or peripheral blood was used as reference. DNA and RNA were simultaneously extracted from the same sample with AllPrep (Qiagen) and *mir*Vana (Ambion) kits after homogenizing the tissues with a ribonuclease-free pestle (VWR) and a QIAshredder column (Qiagen) as detailed in (*47*). RNA quality was inspected with an Agilent 2100 Bioanalyzer.

Gene expression analyses

RNA samples were labeled with biotin and hybridized to Affymetrix Human Genome U133 Plus 2.0 arrays by the University of Texas Southwestern Microarray Core using standard procedures. CEL intensity files were analyzed as previously described (*65*). Probe sets with nonspecific hybridization (10,588, 19%) were discarded. Differences in gene expression between tumors and tumorgrafts were assessed with *t* tests and a Benjamini and Hochberg false discovery rate (FDR) correction (*66*). Probe sets with an FDR $q < 0.05$ and upregulated at least 1.5-fold in tumors versus tumorgrafts were subtracted (2443 probe sets, 4%). These probe sets were analyzed with Ingenuity Pathways Analysis (IPA). Probe sets were also analyzed with principal components and unsupervised hierarchical clustering with Euclidean dissimilarity and an average linkage method in Partek Genomics Suite.

Copy number analyses

DNA samples were hybridized to Affymetrix SNP Arrays 6.0 by the Genome Science Resource (Vanderbilt University) by standard procedures. The CEL intensity files were quantile-normalized with Partek Genomics Suite adjusting for fragment length and probe sequence without background correction as in (*47*). Briefly, paired copy numbers were calculated from intensities for all samples except for TG143, for which a reference copy number baseline from Partek was used, because paired normal was unavailable. Unsupervised hierarchical clustering for 1.8 million markers was computed with Euclidean dissimilarity and an average linkage method. Copy numbers were adjusted for local GC content and were segmented with the circular binary segmentation (CBS) algorithm (*67*) using the DNAcopy package of R/Bioconductor. Segmented copy numbers were displayed with the Integrative Genomics Viewer (Broad Institute). Genotypes were obtained from Affymetrix Genotyping Console 4.0 and used for calculating the allele-specific copy number of each sample in Partek Genomics Suite.

Mutation analyses

Bidirectional Sanger DNA sequencing was performed on genomic DNA from tumors and tumorgrafts by Beckman Coulter Genomics with proprietary primers. Point mutations and indels were identified in chromatograms with Mutation Surveyor v3.30 and v3.98. Mutations within seven nucleotides before or after an exon were considered to affect splicing sites. Mutations are fully detailed in (*47*). Deep sequencing of the *TSC1* mutation was carried out on the Illumina platform by direct amplicon sequencing. *TSC1* sequences were amplified with *TSC1* primers (forward, 5′-CACATCATTGCTGTCTTTATTT; reverse, 5′-CCAACTCTGGACAACATTCTAT) and including common adaptor sequences (forward, 5′-ACACGACGCTCTTCCGATCT-*TSC1*; reverse, 5′-GACGTGTGCTCTTCCGATCT-*TSC1*). Adaptor sequences were used as priming sites in a second polymerase chain reaction (PCR), where oligo sequences converted PCR products into "sequencer ready" templates by the addition of sequences required for clustering, sequencing, and indexing.

PK analyses

PK analyses were performed on 6- to 8-week-old male NOD/SCID mice. PK parameters were calculated in sparse sampling mode with the noncompartmental analysis tool of WinNonlin (Pharsight Corporation). Sirolimus (LC Laboratories) was administered at 0.5 mg/kg intraperitoneally. The compound was dissolved in 5% ethanol, 5% polyethylene glycol 400 (PEG400), 5% Tween 80, and 85% of a 5% dextrose (D5W) solution. Mice were killed at varying times after treatment by CO_2 inhalation, whole blood was drawn with an EDTA coated syringe, 100 µl of whole blood was mixed with 50 µl of 0.2 M zinc sulfate, and 150 µl of 10 mM ammonium acetate in methanol + 0.1% formic acid containing 60 ng per sample of *N*-benzylbenzamide internal standard (IS) was added. After mixing and a 10-min incubation at room temperature, samples were cleared twice by centrifugation and subsequently evaluated by liquid chromatography–tandem mass spectrometry (LC-MS/MS) with an Applied Biosystems/MDS Sciex 3200-QTRAP coupled to a Shimadzu Prominence LC. Standards, prepared by spiking fresh whole blood from uninjected NOD/SCID mice with varying concentrations of sirolimus, were processed following the same procedure. Chromatography conditions were as follows: Buffer A consisted of 10 mM ammonium acetate in water + 0.1% formic acid and Buffer B consisted of 10 mM ammonium acetate in methanol + 0.1% formic acid. The column flow rate was 1.5 ml/min using an Agilent C18 XDB, 5 µm packing, 50 × 4.6 mm size column. The gradient conditions were 0.01 to 1.0 min 100% A, 1.0 to 1.5 min gradient to 100% B, 1.5 to 3.0 min 100% B, 3.0 to 3.1 min gradient to 0% B, 3.1 to 4.1 100% A. Sirolimus was detected in multiple reaction monitoring (MRM) mode by following the precursor to fragment ion transition 931.3 to 864.4. *N*-benzylbenzamide (transition 212.1 to 91.1) was used as an IS. Instrument settings for sirolimus were as follows: dwell time 150 ms, declustering potential (DP) 31 V, entrance potential (EP) 6.5 V, collision cell entrance potential (CEP) 40 V, collision energy (CE) 29 V, cell exit potential (CXP) 10 V, curtain gas (CUR) 30, collision activation dissociation (CAD) med, IS 4500 V, temperature (TEM) 400°C, ion source gas 1 (GS1) 60 psi, ion source gas 2 (GS2) 40 psi. A value three times above the signal obtained from blank whole blood was designated as the limit of detection (LOD). The limit of quantitation (LOQ) was defined as the lowest concentration at which back calculation yielded a concentration within 20% of theoretical and which was above the LOD. The LOQ for sirolimus was 1 ng/ml. In general, back

calculation of points yielded values within 15% of theoretical over five orders of magnitude (1 to 10,000 ng/ml).

Sunitinib malate (Pfizer) was administered at 10 mg/kg by oral gavage in 0.2 ml. The compound was resuspended in 0.5% (w/v) carboxymethylcellulose (CMC) in D5W, pH 7.2. Various times after dose, animals were killed by CO_2 inhalation, blood was collected with an acid citrate dextrose–coated syringe by cardiac puncture, and plasma was isolated by centrifugation. Plasma (100 μl) was precipitated with 400 μl of acetonitrile containing 40 ng per sample of *N*-benzylbenzamide IS. After clearing by centrifugation, 450 μl of supernatant was lyophilized and resuspended in 180 μl of 50:50 acetonitrile/water with 0.1% formic acid. Standards, prepared by spiking blank mouse plasma (Bioreclamation Inc.) with varying concentrations of sunitinib malate and its active metabolite *N*-desethyl sunitinib, were processed following the same procedure used for samples. Chromatography conditions were as follows. Buffer A consisted of water + 0.1% formic acid and Buffer B consisted of acetonitrile + 0.1% formic acid. The column flow rate was 1.5 ml/min using an Agilent C18 XDB, 5 μm packing, 50 × 4.6 mm size column. The gradient conditions were 0.01 to 1.5 min 100% A, 1.5 to 2.0 min gradient to 100% B, 2.0 to 3.5 min 100% B, 3.5 to 3.6 min gradient to 0% B, 3.6 to 5.0 min 100% A. Sunitinib was detected in MRM mode by following the precursor to fragment ion transition 399.1 to 283.2. Instrument settings for sunitinib were as follows: dwell time 150 ms, DP 41 V, EP 4.5 V, CEP 24 V, CE 33 V, CXP 4 V, CUR 45, CAD med, IS 4500 V, TEM 650°C, GS1 60 psi, GS2 45 psi. Desethyl sunitinib was detected in MRM mode by following the precursor to fragment ion transition 371.0 to 326.2. Instrument settings for *N*-desethyl sunitinib were as follows: dwell time 150 ms, DP 31 V, EP 5 V, CEP 16 V, CE 21 V, CXP 4 V, CUR 45, CAD med, IS 4500 V, TEM 650°C, GS1 60 psi, GS2 45 psi. A value three times above the signal obtained from blank plasma was designated as LOD. The LOQ was defined as the lowest concentration at which back calculation yielded a concentration within 20% of theoretical and which was above the LOD. The LOQ for both sunitinib and desethyl sunitinib was 1 ng/ml. In general, back calculation of points yielded values within 15% of theoretical over four orders of magnitude (1 to 1000 ng/ml).

Erlotinib (LC Laboratories) was administered at 12.5 mg/kg by oral gavage in 0.2 ml. The compound was dissolved in 5% ethanol, 0.5% Tween 80, 94.5% of a 0.3% (w/v) CMC in 0.174 M sodium acetate/acetic acid, pH 4.0. At various times after treatment, animals were killed by CO_2 inhalation, blood was collected with an acid citrate dextrose–coated syringe by cardiac puncture, and plasma was isolated by centrifugation. Plasma (100 μl) was precipitated with 200 μl of methanol containing 30 ng per sample of *N*-benzylbenzamide IS and 0.1% formic acid. After clearing by centrifugation, samples were analyzed by LC-MS/MS with an Applied Biosystems/MDS Sciex 3200-QTRAP coupled to a Shimadzu Prominence LC. Standards prepared by spiking blank mouse plasma (Bioreclamation Inc.) with varying concentrations of erlotinib and *O*-desmethyl-erlotinib were processed following the same procedure used for samples. Chromatography conditions were as follows. Buffer A consisted of water + 0.1% formic acid and Buffer B consisted of methanol + 0.1% formic acid. The column flow rate was 1.5 ml/min using an Agilent C18 XDB, 5 μm packing, 50 × 4.6 mm size column. The gradient conditions were 0.01 to 1.2 min 100% A, 1.2 to 2.5 min gradient to 100% B, 2.5 to 3.5 min 100% B, 3.5 to 3.6 min gradient to 0% B, 3.6 to 5.0 min 100% A. Erlotinib was detected in MRM mode by following the precursor to fragment ion transition 394.2 to 278.2. *O*-desmethyl-erlotinib was detected as the 380.1 to 278.1 transition. *N*-benzylbenzamide (transition 212.1 to 91.1) was used as an IS. Instrument settings for erlotinib were as follows: dwell time 150 ms, DP 56 V, EP 5 V, CEP 18 V, CE 45 V, CXP 4 V, CUR 45, CAD med, IS 4500 V, TEM 650°C, GS1 60 psi, GS2 45 psi. Settings for desmethyl erlotinib were as follows: dwell time 150 ms, DP 56 V, EP 5 V, CEP 18 V, CE 45 V, CXP 4 V, CUR 45, CAD med, IS 4500 V, TEM 650°C, GS1 60 psi, GS2 45 psi. A value three times above the signal obtained from blank plasma was designated as LOD. The LOQ was defined as the lowest concentration at which back calculation yielded a concentration within 20% of theoretical and which was above the LOD. The LOQ for both erlotinib and *O*-desmethyl-erlotinib was 0.5 ng/ml. In general, back calculation of points yielded values within 15% of theoretical over four orders of magnitude (0.5 to 1000 ng/ml).

Dovitinib (LC Laboratories) was administered at 30 mg/kg by oral gavage in 0.2 ml. The compound was dissolved in 20 mM lactic acid in D5W. Various times after treatment, animals were killed by CO_2 inhalation, blood was collected with an acid citrate dextrose–coated syringe by cardiac puncture, and plasma was isolated by centrifugation. Plasma (100 μl) was precipitated with 200 μl of acetonitrile containing 80 ng per sample of *N*-benzylbenzamide IS. After clearing by centrifugation, 250 μl of supernatant was mixed with 250 μl of dH_20 containing 0.2% formic acid. Samples were analyzed by LC-MS/MS with an Applied Biosystems/MDS Sciex 3200-QTRAP coupled to a Shimadzu Prominence LC. Standards prepared by spiking blank mouse plasma (Bioreclamation Inc.) with varying concentrations of dovitinib were processed following the same procedure used for samples. Chromatography conditions were as follows. Buffer A consisted of water + 0.1% formic acid and Buffer B consisted of methanol + 0.1% formic acid. The column flow rate was 1.5 ml/min using an Agilent C18 XDB, 5 μm packing, 50 × 4.6 mm size column. The gradient conditions were 0.01 to 1.5 min 100% A, 1.5 to 2.0 min gradient to 100% B, 2.0 to 3.5 min 100% B, 3.5 to 3.6 min gradient to 0% B, 3.6 to 5.0 min 100% A. Dovitinib was detected in MRM mode by following the precursor to fragment ion transition 393.1 to 336.2. *N*-benzylbenzamide (transition 212.1 to 91.1) was used as an IS. Instrument settings for dovitinib were as follows: dwell time 150 ms, DP 71 V, EP 9 V, CEP 18 V, CE 39 V, CXP 4 V, CUR 45, CAD med, IS 4500 V, TEM 650°C, GS1 60 psi, GS2 45 psi. A value three times above the signal obtained from blank plasma was designated as LOD. The LOQ was defined as the lowest concentration at which back calculation yielded a concentration within 20% of theoretical and which was above the LOD. The LOQ for dovitinib was 5 ng/ml. In general, back calculation of points yielded values within 15% of theoretical over four orders of magnitude (5 to 5000 ng/ml).

Drug trials

About 64 mm^3 fragments of tissue from stably growing orthotopic tumorgrafts were implanted subcutaneously in 4- to 6-week-old mice. When tumor volumes reached 250 to 300 mm^3, mice were segregated into appropriate treatment groups (three to five mice per group) on the basis of (i) tumor volume, (ii) growth rate, and (iii) mouse weight. Erlotinib (LC Laboratories) was administered by oral gavage every 12 hours at 12.5 mg/kg in 5% ethanol, 0.5% Tween 80, 94.5% of a 0.3% (w/v) CMC (Sigma-Aldrich) in 0.174 M sodium acetate/acetic acid (pH 4.0). Sirolimus (LC Laboratories) was administered by intraperitoneal injection every 48 hours at 0.5 mg/kg in 5% ethanol, 5% PEG400, 5% Tween 80, and 85% D5W. Vehicle (5% ethanol, 5% PEG400, 5% Tween 80, 85% D5W) was administered by intraperitoneal injection every 48 hours. Sunitinib (Pfizer, LC Laboratories) was administered by oral

gavage every 12 hours at 10 mg/kg in 0.5% CMC in D5W. Dovitinib (LC Laboratories) was administered at 30 mg/kg by oral gavage in 20 mM lactic acid in D5W. Tumor dimensions were measured twice a week with a digital caliper, and tumor volume was calculated by the following formula: tumor volume = $l \times w \times h$, where l is the largest dimension of the tumor, w is the largest diameter perpendicular to l, and h is maximal height of the tumor. Weekly weights were taken and treatment dose was modified accordingly. Mice were typically killed after 4 weeks of treatment, or earlier if they became sick (for example, hypercalcemia), or if tumors became too large from drug trial mice.

Immunohistochemistry

Paraffin-embedded sections were cut and stained with phospho-S6 antibody $S^{240/244}$ (1:100) (Cell Signaling) as described (*40*). Immunostained slides were evaluated independently by two investigators (S.S. and P.K.) who were blinded to clinicopathologic data. Quantitation was performed by P.K. according to the following scale: 1+ (weak), 2+ (moderate), 3+ (strong), and 4+ (very strong), and percentage of tumor cells with cytoplasmic (p-S6) staining: no staining (0), 1 to 24% (1), 25 to 49% (2), 50 to 74% (3), and >75% (4). The product of staining intensity and the percentage of positive cells was used for statistical analysis.

Statistical analyses

The association of specific pathological characteristics and tumor engraftment was evaluated with Fisher's exact test for categorical variables and Student's t test for continuous variables. Outcome analyses excluded the liposarcoma (TG147). Treatment effects on tumor growth were evaluated with a linear mixed model assuming an AR(1) covariance structure. For time-to-event outcome, a log-rank test was used. For deceased patients, when the date of demise was not available, the date of the last encounter was used. Reported P values are two-sided and not adjusted for multiple comparisons unless otherwise indicated. Statistical analyses were performed with SAS 9.2 for Windows (SAS Institute Inc.) and SPSS Statistics 17.0. For statistical analyses of microarray data, please see the corresponding sections.

SUPPLEMENTARY MATERIALS

www.sciencetranslationalmedicine.org/cgi/content/full/4/137/137ra75/DC1

Fig. S1. Evaluation of the effects of implantation site (orthotopically versus subcutaneous) and passage on treatment for tumorgraft line TG164.

Fig. S2. Sunitinib, sirolimus, and erlotinib drug trials by individual tumorgraft line.

Fig. S3. Dovitinib drug trials by tumorgraft line including a papillary line (TG121).

Fig. S4. Treatment effects on mouse weights.

Table S1. Histological evaluation of tumor and corresponding tumorgraft cohort.

Table S2. Overrepresented Ingenuity Pathways corresponding to probe sets up-regulated in tumors over tumorgrafts.

Table S3. Genes differentially expressed in RCC tumors. (Excel file)

Table S4. Overrepresented Ingenuity Canonical Pathways in RCC compared to normal renal cortices before and after immune/stroma signature subtraction.

Table S5. Deep sequencing of the *TSC1* IVS363+5G>T mutation (TG22).

REFERENCES AND NOTES

1. I. Kola, J. Landis, Can the pharmaceutical industry reduce attrition rates? *Nat. Rev. Drug Discov.* **3**, 711–715 (2004).
2. A. Ocana, A. Pandiella, L. L. Siu, I. F. Tannock, Preclinical development of molecular-targeted agents for cancer. *Nat. Rev. Clin. Oncol.* **8**, 200–209 (2010).
3. W. N. Hait, Anticancer drug development: The grand challenges. *Nat. Rev. Drug Discov.* **9**, 253–254 (2010).
4. M. Suggitt, M. C. Bibby, 50 Years of preclinical anticancer drug screening: Empirical to target-driven approaches. *Clin. Cancer Res.* **11**, 971–981 (2005).
5. W. R. Sellers, A blueprint for advancing genetics-based cancer therapy. *Cell* **147**, 26–31 (2011).
6. H. H. Fiebig, A. Maier, A. M. Burger, Clonogenic assay with established human tumour xenografts: Correlation of in vitro to in vivo activity as a basis for anticancer drug discovery. *Eur. J. Cancer* **40**, 802–820 (2004).
7. J. K. Peterson, P. J. Houghton, Integrating pharmacology and in vivo cancer models in preclinical and clinical drug development. *Eur. J. Cancer* **40**, 837–844 (2004).
8. E. A. Sausville, A. M. Burger, Contributions of human tumor xenografts to anticancer drug development. *Cancer Res.* **66**, 3351–3354 (2006).
9. J. Lee, S. Kotliarova, Y. Kotliarov, A. Li, Q. Su, N. M. Donin, S. Pastorino, B. W. Purow, N. Christopher, W. Zhang, J. K. Park, H. A. Fine, Tumor stem cells derived from glioblastomas cultured in bFGF and EGF more closely mirror the phenotype and genotype of primary tumors than do serum-cultured cell lines. *Cancer Cell* **9**, 391–403 (2006).
10. C. Grisanzio, A. Seeley, M. Chang, M. Collins, A. Di Napoli, S. C. Cheng, A. Percy, R. Beroukhim, S. Signoretti, Orthotopic xenografts of RCC retain histological, immunophenotypic and genetic features of tumours in patients. *J. Pathol.* **225**, 212–221 (2011).
11. E. Angevin, L. Glukhova, C. Pavon, A. Chassevent, M. J. Terrier-Lacombe, A. F. Goguel, J. Bougaran, P. Ardouin, B. H. Court, J. L. Perrin, G. Vallancien, F. Triebel, B. Escudier, Human renal cell carcinoma xenografts in SCID mice: Tumorigenicity correlates with a poor clinical prognosis. *Lab. Invest.* **79**, 879–888 (1999).
12. B. Maurer-Schultze, I. D. Bassukas, M. Böswald, M. Harasim, Cell proliferation in human tumours growing in nude mice: Renal cell carcinomas, larynx and hypopharynx carcinomas. *J. Cancer Res. Clin. Oncol.* **118**, 255–268 (1992).
13. W. T. Knöfel, U. Otto, H. Baisch, G. Klöppel, Stability of human renal cell carcinomas during long term serial transplantation into nude mice: Histopathology, nuclear grade, mitotic rate, and DNA content in thirty tumors. *Cancer Res.* **47**, 221–224 (1987).
14. R. V. Clayman, R. S. Figenshau, A. Bear, C. Limas, Transplantation of human renal carcinomas into athymic mice. *Cancer Res.* **45**, 2650–2653 (1985).
15. L. Kopper, E. Magyarosy, P. Nagy, K. Lapis, I. Számel, S. Eckhardt, S. Csata, G. Wabrosch, D. Répássy, Renal cell carcinoma—Xenotransplantation into immuno-suppressed mice. *Oncology* **41**, 19–24 (1984).
16. H. Baisch, U. Otto, G. Klöppel, Long-term serial transplantation of 30 different human renal cell carcinomas into NMRI (nu/nu) mice: Flow cytometric, histologic, and growth studies. *J. Natl. Cancer Inst.* **76**, 269–276 (1986).
17. J. E. Talmadge, R. K. Singh, I. J. Fidler, A. Raz, Murine models to evaluate novel and conventional therapeutic strategies for cancer. *Am. J. Pathol.* **170**, 793–804 (2007).
18. R. M. Hoffman, Orthotopic metastatic mouse models for anticancer drug discovery and evaluation: A bridge to the clinic. *Invest. New Drugs* **17**, 343–359 (1999).
19. I. J. Fidler, Critical factors in the biology of human cancer metastasis: Twenty-eighth G.H.A. Clowes memorial award lecture. *Cancer Res.* **50**, 6130–6138 (1990).
20. J. Brugarolas, Renal-cell carcinoma—Molecular pathways and therapies. *N. Engl. J. Med.* **356**, 185–187 (2007).
21. M. M. Baldewijns, I. J. van Vlodrop, L. J. Schouten, P. M. Soetekouw, A. P. de Bruine, M. van Engeland, Genetics and epigenetics of renal cell cancer. *Biochim. Biophys. Acta* **1785**, 133–155 (2008).
22. M. L. Nickerson, E. Jaeger, Y. Shi, J. A. Durocher, S. Mahurkar, D. Zaridze, V. Matveev, V. Janout, H. Kollarova, V. Bencko, M. Navratilova, N. Szeszenia-Dabrowska, D. Mates, A. Mukeria, I. Holcatova, L. S. Schmidt, J. R. Toro, S. Karami, R. Hung, G. F. Gerard, W. M. Linehan, M. Merino, B. Zbar, P. Boffetta, P. Brennan, N. Rothman, W. H. Chow, F. M. Waldman, L. E. Moore, Improved identification of von Hippel-Lindau gene alterations in clear cell renal tumors. *Clin. Cancer Res.* **14**, 4726–4734 (2008).
23. W. G. Kaelin Jr., The von Hippel–Lindau tumour suppressor protein: O_2 sensing and cancer. *Nat. Rev. Cancer* **8**, 865–873 (2008).
24. A. J. Majmundar, W. J. Wong, M. C. Simon, Hypoxia-inducible factors and the response to hypoxic stress. *Mol. Cell* **40**, 294–309 (2010).
25. N. Ferrara, VEGF and the quest for tumour angiogenesis factors. *Nat. Rev. Cancer* **2**, 795–803 (2002).
26. A. Armulik, A. Abramsson, C. Betsholtz, Endothelial/pericyte interactions. *Circ. Res.* **97**, 512–523 (2005).
27. N. Ferrara, K. J. Hillan, H. P. Gerber, W. Novotny, Discovery and development of bevacizumab, an anti-VEGF antibody for treating cancer. *Nat. Rev. Drug Discov.* **3**, 391–400 (2004).
28. J. C. Yang, L. Haworth, R. M. Sherry, P. Hwu, D. J. Schwartzentruber, S. L. Topalian, S. M. Steinberg, H. X. Chen, S. A. Rosenberg, A randomized trial of bevacizumab, an anti-vascular endothelial growth factor antibody, for metastatic renal cancer. *N. Engl. J. Med.* **349**, 427–434 (2003).
29. B. Escudier, J. Bellmunt, S. Négrier, E. Bajetta, B. Melichar, S. Bracarda, A. Ravaud, S. Golding, S. Jethwa, V. Sneller, Phase III trial of bevacizumab plus interferon alfa-2a in patients with metastatic renal cell carcinoma (AVOREN): Final analysis of overall survival. *J. Clin. Oncol.* **28**, 2144–2150 (2010).

30. B. I. Rini, S. Halabi, J. E. Rosenberg, W. M. Stadler, D. A. Vaena, L. Archer, J. N. Atkins, J. Picus, P. Czaykowski, J. Dutcher, E. J. Small, Phase III trial of bevacizumab plus interferon alfa versus interferon alfa monotherapy in patients with metastatic renal cell carcinoma: Final results of CALGB 90206. *J. Clin. Oncol.* **28**, 2137–2143 (2010).
31. B. Escudier, T. Eisen, W. M. Stadler, C. Szczylik, S. Oudard, M. Siebels, S. Negrier, C. Chevreau, E. Solska, A. A. Desai, F. Rolland, T. Demkow, T. E. Hutson, M. Gore, S. Freeman, B. Schwartz, M. Shan, R. Simantov, R. M. Bukowski; TARGET Study Group, Sorafenib in advanced clear-cell renal-cell carcinoma. *N. Engl. J. Med.* **356**, 125–134 (2007).
32. R. J. Motzer, T. E. Hutson, P. Tomczak, M. D. Michaelson, R. M. Bukowski, O. Rixe, S. Oudard, S. Negrier, C. Szczylik, S. T. Kim, I. Chen, P. W. Bycott, C. M. Baum, R. A. Figlin, Sunitinib versus interferon alfa in metastatic renal-cell carcinoma. *N. Engl. J. Med.* **356**, 115–124 (2007).
33. C. N. Sternberg, I. D. Davis, J. Mardiak, C. Szczylik, E. Lee, J. Wagstaff, C. H. Barrios, P. Salman, O. A. Gladkov, A. Kavina, J. J. Zarbá, M. Chen, L. McCann, L. Pandite, D. F. Roychowdhury, R. E. Hawkins, Pazopanib in locally advanced or metastatic renal cell carcinoma: Results of a randomized phase III trial. *J. Clin. Oncol.* **28**, 1061–1068 (2010).
34. B. I. Rini, B. Escudier, P. Tomczak, A. Kaprin, C. Szczylik, T. E. Hutson, M. D. Michaelson, V. A. Gorbunova, M. E. Gore, I. G. Rusakov, S. Negrier, Y. C. Ou, D. Castellano, H. Y. Lim, H. Uemura, J. Tarazi, D. Cella, C. Chen, B. Rosbrook, S. Kim, R. J. Motzer, Comparative effectiveness of axitinib versus sorafenib in advanced renal cell carcinoma (AXIS): A randomised phase 3 trial. *Lancet* **378**, 1931–1939 (2011).
35. J. B. Brugarolas, F. Vazquez, A. Reddy, W. R. Sellers, W. G. Kaelin Jr., TSC2 regulates VEGF through mTOR-dependent and -independent pathways. *Cancer Cell* **4**, 147–158 (2003).
36. A. J. Pantuck, D. B. Seligson, T. Klatte, H. Yu, J. T. Leppert, L. Moore, T. O'Toole, J. Gibbons, A. S. Belldegrun, R. A. Figlin, Prognostic relevance of the mTOR pathway in renal cell carcinoma: Implications for molecular patient selection for targeted therapy. *Cancer* **109**, 2257–2267 (2007).
37. V. A. Robb, M. Karbowniczek, A. J. Klein-Szanto, E. P. Henske, Activation of the mTOR signaling pathway in renal clear cell carcinoma. *J. Urol.* **177**, 346–352 (2007).
38. T. Abou Youssif, M. A. Fahmy, I. H. Koumakpayi, F. Ayala, S. Al Marzooqi, G. Chen, P. Tamboli, J. Squire, S. Tanguay, K. Sircar, The mammalian target of rapamycin pathway is widely activated without *PTEN* deletion in renal cell carcinoma metastases. *Cancer* **117**, 290–300 (2011).
39. F. Lin, P. L. Zhang, X. J. Yang, J. W. Prichard, M. Lun, R. E. Brown, Morphoproteomic and molecular concomitants of an overexpressed and activated mTOR pathway in renal cell carcinomas. *Ann. Clin. Lab. Sci.* **36**, 283–293 (2006).
40. B. Kucejova, S. Peña-Llopis, T. Yamasaki, S. Sivanand, T. A. Tran, S. Alexander, N. C. Wolff, Y. Lotan, X. J. Xie, W. Kabbani, P. Kapur, J. Brugarolas, Interplay between pVHL and mTORC1 pathways in clear-cell renal cell carcinoma. *Mol. Cancer Res.* **9**, 1255–1265 (2011).
41. G. Hudes, M. Carducci, P. Tomczak, J. Dutcher, R. Figlin, A. Kapoor, E. Staroslawska, J. Sosman, D. McDermott, I. Bodrogi, Z. Kovacevic, V. Lesovoy, I. G. Schmidt-Wolf, O. Barbarash, E. Gokmen, T. O'Toole, S. Lustgarten, L. Moore, R. J. Motzer; Global ARCC Trial, Temsirolimus, interferon alfa, or both for advanced renal-cell carcinoma. *N. Engl. J. Med.* **356**, 2271–2281 (2007).
42. R. J. Motzer, B. Escudier, S. Oudard, T. E. Hutson, C. Porta, S. Bracarda, V. Grunwald, J. A. Thompson, R. A. Figlin, N. Hollaender, G. Urbanowitz, W. J. Berg, A. Kay, D. Lebwohl, A. Ravaud; RECORD-1 Study Group, Efficacy of everolimus in advanced renal cell carcinoma: A double-blind, randomised, placebo-controlled phase III trial. *Lancet* **372**, 449–456 (2008).
43. S. A. Hahn, A. B. Seymour, A. T. Hoque, M. Schutte, L. T. da Costa, M. S. Redston, C. Caldas, C. L. Weinstein, A. Fischer, C. J. Yeo, R. H. Hruban, S. E. Kern, Allelotype of pancreatic adenocarcinoma using xenograft enrichment. *Cancer Res.* **55**, 4670–4675 (1995).
44. M. Chen, Y. Ye, H. Yang, P. Tamboli, S. Matin, N. M. Tannir, C. G. Wood, J. Gu, X. Wu, Genome-wide profiling of chromosomal alterations in renal cell carcinoma using high-density single nucleotide polymorphism arrays. *Int. J. Cancer* **125**, 2342–2348 (2009).
45. R. Beroukhim, C. H. Mermel, D. Porter, G. Wei, S. Raychaudhuri, J. Donovan, J. Barretina, J. S. Boehm, J. Dobson, M. Urashima, K. T. Mc Henry, R. M. Pinchback, A. H. Ligon, Y. J. Cho, L. Haery, H. Greulich, M. Reich, W. Winckler, M. S. Lawrence, B. A. Weir, K. E. Tanaka, D. Y. Chiang, A. J. Bass, A. Loo, C. Hoffman, J. Prensner, T. Liefeld, Q. Gao, D. Yecies, S. Signoretti, E. Maher, F. J. Kaye, H. Sasaki, J. E. Tepper, J. A. Fletcher, J. Tabernero, J. Baselga, M. S. Tsao, F. Demichelis, M. A. Rubin, P. A. Janne, M. J. Daly, C. Nucera, R. L. Levine, B. L. Ebert, S. Gabriel, A. K. Rustgi, C. R. Antonescu, M. Ladanyi, A. Letai, L. A. Garraway, M. Loda, D. G. Beer, L. D. True, A. Okamoto, S. L. Pomeroy, S. Singer, T. R. Golub, E. S. Lander, G. Getz, W. R. Sellers, M. Meyerson, The landscape of somatic copy-number alteration across human cancers. *Nature* **463**, 899–905 (2010).
46. V. R. Dondeti, B. Wubbenhorst, P. Lal, J. D. Gordan, K. D'Andrea, E. F. Attiyeh, M. C. Simon, K. L. Nathanson, Integrative genomic analyses of sporadic clear cell renal cell carcinoma define disease subtypes and potential new therapeutic targets. *Cancer Res.* **72**, 112–121 (2012).
47. S. Peña-Llopis, S. Vega-Rubin-de-Celis, A. Liao, N. Leng, A. Pavía-Jiménez, S. Wang, T. Yamasaki, L. Zhrebker, S. Sivanand, P. Spence, L. Kinch, T. Hambuch, S. Jain, Y. Lotan, V. Margulis, A. I. Sagalowsky, P. B. Summerour, W. Kabbani, S. W. Wendy Wong, N. Grishin, M. Laurent, X.-J. Xie, C. Haudenschild, M. T. Ross, D. R. Bentley, P. Kapur, J. Brugarolas, BAP1 loss defines a new class of renal cell carcinoma. *Nat. Genet.* 10.1038/ng.2323 (2012).
48. M. Gerlinger, A. J. Rowan, S. Horswell, J. Larkin, D. Endesfelder, E. Gronroos, P. Martinez, N. Matthews, A. Stewart, P. Tarpey, I. Varela, B. Phillimore, S. Begum, N. Q. McDonald, A. Butler, D. Jones, K. Raine, C. Latimer, C. R. Santos, M. Nohadani, A. C. Eklund, B. Spencer-Dene, G. Clark, L. Pickering, G. Stamp, M. Gore, Z. Szallasi, J. Downward, P. A. Futreal, C. Swanton, Intratumor heterogeneity and branched evolution revealed by multiregion sequencing. *N. Engl. J. Med.* **366**, 883–892 (2012).
49. L. Ding, M. J. Ellis, S. Li, D. E. Larson, K. Chen, J. W. Wallis, C. C. Harris, M. D. McLellan, R. S. Fulton, L. L. Fulton, R. M. Abbott, J. Hoog, D. J. Dooling, D. C. Koboldt, H. Schmidt, J. Kalicki, Q. Zhang, L. Chen, L. Lin, M. C. Wendl, J. F. McMichael, V. J. Magrini, L. Cook, S. D. McGrath, T. L. Vickery, E. Appelbaum, K. Deschryver, S. Davies, T. Guintoli, L. Lin, R. Crowder, Y. Tao, J. E. Snider, S. M. Smith, A. F. Dukes, G. E. Sanderson, C. S. Pohl, K. D. Delehaunty, C. C. Fronick, K. A. Pape, J. S. Reed, J. S. Robinson, J. S. Hodges, W. Schierding, N. D. Dees, D. Shen, D. P. Locke, M. E. Wiechert, J. M. Eldred, J. B. Peck, B. J. Oberkfell, J. T. Lolofie, F. Du, A. E. Hawkins, M. D. O'Laughlin, K. E. Bernard, M. Cunningham, G. Elliott, M. D. Mason, D. M. Thompson Jr., J. L. Ivanovich, P. J. Goodfellow, C. M. Perou, G. M. Weinstock, R. Aft, M. Watson, T. J. Ley, R. K. Wilson, E. R. Mardis, Genome remodelling in a basal-like breast cancer metastasis and xenograft. *Nature* **464**, 999–1005 (2010).
50. M. B. Atkins, M. Hidalgo, W. M. Stadler, T. F. Logan, J. P. Dutcher, G. R. Hudes, Y. Park, S. H. Liou, B. Marshall, J. P. Boni, G. Dukart, M. L. Sherman, Randomized phase II study of multiple dose levels of CCI-779, a novel mammalian target of rapamycin kinase inhibitor, in patients with advanced refractory renal cell carcinoma. *J. Clin. Oncol.* **22**, 909–918 (2004).
51. E. Raymond, J. Alexandre, S. Faivre, K. Vera, E. Materman, J. Boni, C. Leister, J. Korth-Bradley, A. Hanauske, J. P. Armand, Safety and pharmacokinetics of escalated doses of weekly intravenous infusion of CCI-779, a novel mTOR inhibitor, in patients with cancer. *J. Clin. Oncol.* **22**, 2336–2347 (2004).
52. J. Brugarolas, Y. Lotan, L. Watumull, W. Kabbani, Sirolimus in metatastic renal cell carcinoma. *J. Clin. Oncol.* **26**, 3457–3460 (2008).
53. R. M. Bukowski, F. F. Kabbinavar, R. A. Figlin, K. Flaherty, S. Srinivas, U. Vaishampayan, H. A. Drabkin, J. Dutcher, S. Ryba, Q. Xia, F. A. Scappaticci, D. McDermott, Randomized phase II study of erlotinib combined with bevacizumab compared with bevacizumab alone in metastatic renal cell cancer. *J. Clin. Oncol.* **25**, 4536–4541 (2007).
54. J. P. Boni, C. Leister, G. Bender, V. Fitzpatrick, N. Twine, J. Stover, A. Dorner, F. Immermann, M. E. Burczynski, Population pharmacokinetics of CCI-779: Correlations to safety and pharmacogenomic responses in patients with advanced renal cancer. *Clin. Pharmacol. Ther.* **77**, 76–89 (2005).
55. A. Awada, F. Cardoso, C. Fontaine, L. Dirix, J. De Grève, C. Sotiriou, J. Steinseifer, C. Wouters, C. Tanaka, U. Zoellner, P. Tang, M. Piccart, The oral mTOR inhibitor RAD001 (everolimus) in combination with letrozole in patients with advanced breast cancer: Results of a phase I study with pharmacokinetics. *Eur. J. Cancer* **44**, 84–91 (2008).
56. A. R. Tan, X. Yang, S. M. Hewitt, A. Berman, E. R. Lepper, A. Sparreboom, A. L. Parr, W. D. Figg, C. Chow, S. M. Steinberg, S. L. Bacharach, M. Whatley, J. A. Carrasquillo, J. S. Brahim, S. A. Ettenberg, S. Lipkowitz, S. M. Swain, Evaluation of biologic end points and pharmacokinetics in patients with metastatic breast cancer after treatment with erlotinib, an epidermal growth factor receptor tyrosine kinase inhibitor. *J. Clin. Oncol.* **22**, 3080–3090 (2004).
57. J. J. Raizer, L. E. Abrey, A. B. Lassman, S. M. Chang, K. R. Lamborn, J. G. Kuhn, W. K. Yung, M. R. Gilbert, K. A. Aldape, P. Y. Wen, H. A. Fine, M. Mehta, L. M. Deangelis, F. Lieberman, T. F. Cloughesy, H. I. Robins, J. Dancey, M. D. Prados; North American Brain Tumor Consortium, A phase II trial of erlotinib in patients with recurrent malignant gliomas and nonprogressive glioblastoma multiforme postradiation therapy. *Neuro Oncol.* **12**, 95–103 (2010).
58. R. Anjum, J. Blenis, The RSK family of kinases: Emerging roles in cellular signalling. *Nat. Rev. Mol. Cell Biol.* **9**, 747–758 (2008).
59. S. Trudel, Z. H. Li, E. Wei, M. Wiesmann, H. Chang, C. Chen, D. Reece, C. Heise, A. K. Stewart, CHIR-258, a novel, multitargeted tyrosine kinase inhibitor for the potential treatment of t(4;14) multiple myeloma. *Blood* **105**, 2941–2948 (2005).
60. J. S. Yuen, M. Y. Sim, H. G. Siml, T. W. Chong, W. K. Lau, C. W. Cheng, H. Huynh, Inhibition of angiogenic and non-angiogenic targets by sorafenib in renal cell carcinoma (RCC) in a RCC xenograft model. *Br. J. Cancer* **104**, 941–947 (2011).
61. J. A. Karam, X. Y. Zhang, P. Tamboli, V. Margulis, H. Wang, E. J. Abel, S. H. Culp, C. G. Wood, Development and characterization of clinically relevant tumor models from patients with renal cell carcinoma. *Eur. Urol.* **59**, 619–628 (2011).
62. X. Xu, Y. Hou, X. Yin, L. Bao, A. Tang, L. Song, F. Li, S. Tsang, K. Wu, H. Wu, W. He, L. Zeng, M. Xing, R. Wu, H. Jiang, X. Liu, D. Cao, G. Guo, X. Hu, Y. Gui, Z. Li, W. Xie, X. Sun, M. Shi, Z. Cai, B. Wang, M. Zhong, J. Li, Z. Lu, N. Gu, X. Zhang, L. Goodman, L. Bolund, J. Wang, H. Yang, K. Kristiansen, M. Dean, Y. Li, J. Wang, Single-cell exome sequencing reveals single-nucleotide mutation characteristics of a kidney tumor. *Cell* **148**, 886–895 (2012).
63. T. Yamasaki, T. A. Tran, O. K. Oz, G. V. Raj, R. E. Schwarz, R. J. Deberardinis, X. Zhang, J. Brugarolas, Exploring a glycolytic inhibitor for the treatment of an *FH*-deficient type-2 papillary RCC. *Nat. Rev. Urol.* **8**, 165–171 (2011).
64. B. Kucejova, N. E. Sunny, A. D. Nguyen, R. Hallac, X. Fu, S. Peña-Llopis, R. P. Mason, R. J. Deberardinis, X. J. Xie, R. Debose-Boyd, V. D. Kodibagkar, S. C. Burgess, J. Brugarolas, Uncoupling hypoxia signaling from oxygen sensing in the liver results in hypoketotic hypoglycemic death. *Oncogene* **30**, 2147–2160 (2011).

65. S. Peña-Llopis, S. Vega-Rubin-de-Celis, J. C. Schwartz, N. C. Wolff, T. A. Tran, L. Zou, X. J. Xie, D. R. Corey, J. Brugarolas, Regulation of TFEB and V-ATPases by mTORC1. *EMBO J.* **30**, 3242–3258 (2011).
66. Y. Benjamini, Y. Hochberg, Controlling the false discovery rate: A practical and powerful approach to multiple testing. *J. R. Statist. Soc. B* **57**, 289–300 (1995).
67. A. B. Olshen, E. S. Venkatraman, R. Lucito, M. Wigler, Circular binary segmentation for the analysis of array-based DNA copy number data. *Biostatistics* **5**, 557–572 (2004).
68. S. Faivre, C. Delbaldo, K. Vera, C. Robert, S. Lozahic, N. Lassau, C. Bello, S. Deprimo, N. Brega, G. Massimini, J.-P. Armand, P. Scigalla, E. Raymond, Safety, pharmacokinetic, and antitumor activity of SU11248, a novel oral multitarget tyrosine kinase inhibitor, in patients with cancer. *J. Clin. Oncol.* **24**, 23–35 (2006).
69. E. Angevin, J. A. Lopez, A. Pande, C. Moldovan, M. Shi, J. C. Soria, X. Wang, A. Harzstark, J. Saro, B. Escudier, TKI258 (dovitinib lactate) in metastatic renal cell carcinoma (mRCC) patients refractory to approved targeted therapies: A phase I/II dose finding and biomarker study. *J. Clin. Oncol.* **27**, 15s (2009).
70. K. B. Kim, J. Chesney, D. Robinson, H. Gardner, M. M. Shi, J. M. Kirkwood, Phase I/II and pharmacodynamic study of dovitinib (TKI258), an inhibitor of fibroblast growth factor receptors and VEGF receptors, in patients with advanced melanoma. *Clin. Cancer Res.* **17**, 7451–7461 (2011).

Acknowledgments: We thank all the patients who donated samples. We also thank A. Husain, A. Yadlapalli, and A. Purushotham for technical support; J. Minna for NSCLC tumor cell line; the University of Texas Southwestern tissue resource staff for tissue procurement; Pfizer for providing sunitinib; and all the members of the Brugarolas lab for reviewing the manuscript. **Funding:** This work was supported by the following grants to J.B.: American Cancer Society Research Scholar Grant (115739), RO1CA129387, and Cancer Prevention and Research Institute of Texas (RP101075). N.S.W. and the pharmacokinetic studies were supported in part by P01CA095471 (principal investigator, S. McKnight). The Vevo770 ultrasound was purchased with 1S10RR02564801, and imaging was facilitated by the Small Animal Imaging Research Program supported in part by U24CA126608. The tissue management shared resource is supported in part by the National Cancer Institute (1P30CA142543). S.P.-L. was partially supported by a fellowship of excellence from Generalitat Valenciana (BPOSTDOC06/004). J.B. is a Virginia Murchison Linthicum Scholar in Medical Research at University of Texas Southwestern. The content is solely the responsibility of the authors and does not represent official views from any of the granting agencies. **Author contributions:** S.S. set up and maintained the tumorgraft lines and database, processed tissue for histology and reviewed the slides, was responsible for most of the drug trials, and wrote the first draft of the manuscript. S.P.-L. processed, managed, and extracted nucleic acids from tissues and performed gene expression, DNA copy number and mutational analyses, and the corresponding statistical analyses. H.Z. performed statistical analyses under the supervision of X.-J.X. B.K. assisted with drug trials and immunohistochemistry. P.S. conducted dovitinib drug trials. A.P.-J. processed tissue and helped with tumorgraft colony maintenance. T.Y. helped with imaging studies. D.J.M. performed deep sequencing studies under the supervision of M.T.R. and D.R.B. J.G. obtained consent from patients, and N.C.W. established procedures for tumorgraft processing. L.M. performed all pharmacokinetic analyses under the supervision of N.S.W. who developed protocols for drug preparation and administration. Y.L., G.V.R., A.S., V.M., and J.A.C. performed surgeries and provided tissue samples. P.K. prepared, stained, and analyzed, together with W.K., all histological sections, including immunohistochemical stains. J.B. conceived the study, directed the project, and wrote the manuscript with input from other authors. **Competing interests:** The authors declare that they have no competing interests. **Data and materials availability:** Materials will be shared according to the University's Office for Technology Development policies and Institutional Review Board. Gene expression and SNP arrays were deposited in ArrayExpress under accession IDs E-MTAB-1050 and E-MTAB-1051, respectively.

Submitted 22 December 2011
Accepted 10 April 2012
Published 6 June 2012
10.1126/scitranslmed.3003643

Citation: S. Sivanand, S. Peña-Llopis, H. Zhao, B. Kucejova, P. Spence, A. Pavia-Jimenez, T. Yamasaki, D. J. McBride, J. Gillen, N. C. Wolff, L. Morlock, Y. Lotan, G. V. Raj, A. Sagalowsky, V. Margulis, J. A. Cadeddu, M. T. Ross, D. R. Bentley, W. Kabbani, X.-J. Xie, P. Kapur, N. S. Williams, J. Brugarolas, A validated tumorgraft model reveals activity of dovitinib against renal cell carcinoma. *Sci. Transl. Med.* **4**, 137ra75 (2012).